Improved Shield Tunnel Design Methodology Incorporating Design Robustness

Wenping Gong [1], Hongwei Huang [2], C. Hsein Juang [3]*, Sez Atamturktur [4], Andrew Brownlow [5]

Abstract: This paper presents an improved design methodology for shield tunnels. Here, a new framework for 3-D analysis of shield tunnel *performance* (defined herein as the structural safety and serviceability of each tunnel ring) is developed, which considers the effect of the longitudinal variation of input parameters on the tunnel performance. Within this framework, random fields are used to simulate the longitudinal variation of input parameters, and the 3-D problem of shield tunnel performance is solved through a two-stage solution involving a 1-D model (for tunnel longitudinal behavior) and a 2-D model (for performance of segment rings). Furthermore, the robust design concept is integrated into the design of shield tunnels to guard against the longitudinal variation of tunnel performance caused by the longitudinal variation of input parameters. In the context of robust design, a new measure is developed for determining the robustness of the tunnel performance against the longitudinal variation of noise factors; and then, a multi-objective optimization is performed to optimize the design with respect to the design robustness and the cost efficiency, while satisfying the safety and serviceability requirements. Through an illustrative example, the effectiveness and significance of the improved shield tunnel design methodology is demonstrated.

Keywords: Robust design; shield tunnel; design robustness; multi-objective optimization; longitudinal variation of input parameters.

[1] Research Assistant Professor, Glenn Department of Civil Engineering, Clemson University, Clemson, SC 29634, USA; also affiliated with Department of Geotechnical Engineering, Tongji University, Shanghai 200092, China.

[2] Professor, Key Laboratory of Geotechnical and Underground Engineering of Minister of Education, Tongji University, Shanghai 200092, China; also affiliated with Department of Geotechnical Engineering, Tongji University, Shanghai 200092, China.

[3] Glenn Professor, Glenn Department of Civil Engineering, Clemson University, Clemson, SC 29634, USA (corresponding author). E-mail: HSEIN@clemson.edu

[4] Associate Professor, Glenn Department of Civil Engineering, Clemson University, Clemson, SC 29634, USA.

[5] Research Assistant, Glenn Department of Civil Engineering, Clemson University, Clemson, SC 29634, USA.

Introduction

With the advances of shield-driven machines and tunneling technologies, shield tunneling has become an internationally well-known technology used in the construction of tunnels in urban areas (Gong et al. 2014b). The methodologies for the design of the lining of shield tunnels have remained static over the past few decades. The current design practice still relies on the analysis of a few critical tunnel cross-sections adopting a plane strain assumption, although the analysis methods have evolved from empirical models to mechanics-based models (Wood 1975; ITA 2000; Bobet 2001; Lee et al. 2001; Lee and Ge 2001; Koyama 2003). As the longitudinal length of a shield tunnel is in the hundreds (or thousands) of meters while the diameter is usually less than 15 m, the analysis and design of the shield tunnel should be a three-dimensional (3-D) problem instead of a two-dimensional (2-D) plane strain problem. Furthermore, the longitudinal variation of input parameters (e.g., soil parameters, ground water table, and overburden), caused by the longitudinal variation of tunnel alignment, spatial variation of soil parameters, and nearby tunneling activities, could affect the tunnel performance significantly. The effect of the longitudinal variation of input parameters has not yet been adequately investigated.

Because of the effect of the longitudinal variation of input parameters, the *performance* of a shield tunnel, defined herein as the structural safety and serviceability of each segment ring, may not be correctly reflected in the analysis results of a few "representative" segment rings (or cross-sections). Moreover, the selection of the representative tunnel cross-sections can be quite subjective; different designers may have different selections. Thus, a more rational model for the analysis and design of shield tunnels that considers the longitudinal variation of input parameters is needed. For a shield tunnel with input parameters that are subject to longitudinal variation, its performance cannot be evaluated with certainty. Even if the longitudinal variation of input

parameters can be accurately characterized, which is rarely the case, different segment rings may exhibit different factors of safety, with respect to the structural safety and serviceability. Therefore, an improved design methodology for shield tunnels is proposed in this paper to account for the longitudinal variation of input parameters.

In this paper, a new framework for the shield tunnel performance analysis is first advanced. In which, random fields are used to simulate the longitudinal variation of input parameters, and the input parameters for the tunnel design are first generated with Monte Carlo simulation (MCS). The generated input parameters are then used to analyze the tunnel longitudinal behavior, including tunnel settlement, longitudinal rotation, longitudinal bending moment, and longitudinal shear force. Here the one-dimensional (1-D) finite element method (FEM) based on the Winkler elastic foundation theory (Huang et al. 2015) is used for that analysis. Both the obtained tunnel longitudinal behaviors and the simulated input parameters for the tunnel design are then used to study the structural safety and serviceability of each segment ring. For the analysis of the structural safety and serviceability of segment rings, the two-dimensional (2-D) analytical solution developed in Gong et al. (2015a) is adopted, which explicitly considers both shearing effect (Liao et al. 2005) and flattening effect (Huang et al. 2012). Thus, the 3-D problem of shield tunnel performance is solved with the solution of a 1-D problem (for the tunnel longitudinal behavior) and the solutions of a series of 2-D problems (for the performance of each segment ring).

Furthermore, to reduce the effect of input parameters uncertainty on the tunnel design, the concept of robust design, pioneered by Taguchi (1986) in the field of quality engineering, is adapted herein for robust design of shield tunnels. The robust design concept has been applied to many engineering fields (e.g., Tsui 1992; Chen et al. 1996; Liu et al. 2013; Liu et al. 2014). A

survey of geotechnical applications was provided by Khoshnevisan et al. (2014). Although the subject of robust design of shield tunnels was reported previously (Gong et al. 2014b), it was limited to the design of a single segment ring and the longitudinal variation of input parameters was not investigated. In the present study, the focus is on the design of a tunnel longitudinal structure that consists of a huge number of segment rings, for which explicit consideration of the longitudinal variation of input parameters is necessary. As mentioned previously, different segment rings might exhibit different tunnel performances; thus, the evaluation of the design robustness of a tunnel longitudinal structure could be a significant challenge. The evaluation of the design robustness of a geotechnical system with multi-system responses of concern is much different from that reported in the current robust geotechnical design applications, in which only one or two system responses were investigated (Juang et al. 2013&2014; Wang et al. 2013; Gong et al. 2014b&c; Khoshnevisan et al. 2014&2015).

In the context of robust design, the input parameters are classified into two categories: (a) the design parameters that are subject to easy adjustment or control by the designer, and (b) the noise factors that are associated with the longitudinal variation and that are not easily controlled by the designer. The robust design of a shield tunnel is then implemented as a multi-objective optimization problem, as the design objectives are to satisfy the performance requirements (i.e., structural safety and serviceability), and to increase the cost efficiency and design robustness simultaneously. Note that the design robustness is referred to the insensitivity of the tunnel performance against the unforeseen longitudinal variation of noise factors. As a significant improvement to the previously reported robust geotechnical design methodology (Juang et al. 2013&2014; Wang et al. 2013; Gong et al. 2014b&c; Khoshnevisan et al. 2014&2015), a new robustness measure is formulated in this paper, which enables an efficient consideration of the

longitudinal variation of tunnel performance (due to the existence of the longitudinal variation of noise factors).

In the balance of this paper, the new framework for the shield tunnel performance analysis that considers the longitudinal variation of input parameters is presented, followed by the formulation of the new robustness measure and robust design methodology for shield tunnels. An illustrative example of the improved shield tunnel design methodology is next elucidated to demonstrate its effectiveness and significance.

New Framework for Shield Tunnel Performance Analysis

While it has long been acknowledged that the longitudinal variation of input parameters must be explicitly considered in the analysis and design of shield tunnels (ITA 2000; ATRB 2000; Koyama 2003), a convincing framework for shield tunnel performance analysis that considers the longitudinal variation of input parameters is not available. In this paper, we advance a simple framework for shield tunnel performance analysis. In reference to Figure 1, this framework is outlined as follows.

Step 1: Generating input parameters with Monte Carlo simulation

Random field theory is used herein to model the longitudinal variation (or the spatial variation in the longitudinal domain) of input parameters for the shield tunnel design (e.g., soil parameters, ground water table, and overburden). Random field to simulate the spatial variation (in the longitudinal domain) of tunnel input parameters is used in this context as in geotechnical engineering, in which the spatial variation of soil parameters is often simulated with random fields (Baker 1984; Phoon and Kulhawy 1999; Fenton and Griffiths 2002; Fenton and Griffiths 2003; Cho 2007; Luo et al. 2012). In this paper, the authors use their methods of using the Monte

Carlo simulation (MCS) to generate the tunnel input parameters along the longitudinal direction (see Appendix A for detailed formulations).

Note that a prerequisite for the generation of tunnel input parameters with MCS is the availability of the statistical information (i.e., the mean μ, the coefficient of variation δ, the scale of fluctuation r, and the distribution type) of these input parameters. In practice, the statistical information of these input parameters is estimated using the data from site exploration, published literature, and local experience. Oftentimes, the maximum likelihood estimate method (e.g., Fenton 1999; Gong et al. 2014a) or Bayesian updating method (Wang and Cao 2013; Cao and Wang 2014) can aid in the statistical characterization of input parameters. For illustration, we consider the longitudinal variation of the following input parameters in this study: the vertical ground stiffness (k_v), horizontal ground stiffness (k_h), effective cohesion (c), effective friction angle (ϕ), ground water table (H_w) and ground surcharge (q_0).

Step 2: Analyzing tunnel longitudinal behavior with 1-D FEM solution

Based upon the tunnel input parameters generated in Step 1, including the vertical stiffness of the ground under the tunnel (k_v), ground water table (H_w), and ground surcharge (q_0), the longitudinal behaviors of the shield tunnel, including tunnel settlement (w), longitudinal rotation (θ_L), longitudinal bending moment (M_L) and longitudinal shear force (Q_L), are readily analyzed using the simplified 1-D FEM solution that is developed based upon the Winkler elastic foundation theory (Huang et al. 2015). The schematic diagram of the adopted 1-D FEM model of the shield tunnel is shown in Figure 2. Here, the longitudinal structure of the shield tunnel is modeled as an elastic and continuous beam, and the effect of the longitudinal joints, which are the joints between segment rings, is simulated by a reduction factor of tunnel longitudinal flexural stiffness (Liao et al. 2008). The soil-structure interaction between the tunnel beam and

the ground under the tunnel is modeled with the Winkler model; and the overburden on the tunnel is modeled with the pressure load (see Appendix B for detailed formulations of the 1-D FEM solution of tunnel longitudinal behavior). Here, the vertical ground stiffness (k_v) of the ground under the tunnel can be represented with the coefficient of the vertical subgrade reaction, which may be determined with either the plate-load test data (Lin et al. 1998) or the elastic modulus and Poisson's ratio of the soil determined with laboratory tests (Winkler 1867; Horvath 1983; Sadrekarimi and Akbarzad 2009).

Step 3: Analyzing the performance of the segment ring with 2-D analytical solution

Based upon the tunnel input parameters, specifically the horizontal ground stiffness (k_h), effective cohesion (c), effective friction angle (ϕ), ground water table (H_w) and ground surcharge (q_0) along the longitudinal direction that were generated in Step 1, and the tunnel longitudinal behaviors that were obtained in Step 2, the 2-D analytical solution is readily used to study the performance (i.e., structural safety and serviceability) of the segment ring (Gong et al. 2015a). The schematic diagram of the adopted 2-D analytical solution of the segment ring is plotted in Figure 3 (see Appendix C for detailed load conditions of the segment ring). Here, the shearing effect (Liao et al. 2005) and flattening effect (Huang et al. 2012) are used to study how the tunnel longitudinal behavior affects the performance of the segment ring.

The results of the 2-D analytical solution are the internal forces (i.e., axial force N, bending moment M, and shear force Q) and convergence deformations (i.e., vertical convergence deformation Δ_v and horizontal convergence deformation Δ_h) of the tunnel lining, which are then used to assess the performance of the segment ring. Here, the internal forces are used to calculate the factor of safety with respect to the structural safety, denoted as Fs_1, using the limit state design method (ITA 2000; Gong et al. 2014b); in which, the elastic to plastic behavior of steel

reinforced tunnel segment can be effectively included. The convergence deformations are used to compute the factor of safety with respect to the serviceability, denoted as Fs_2, using the procedure developed by Gong et al. (2014b). As specified in the Chinese metro code (MCPRC 2003), the maximum convergence deformation of the tunnel lining must be controlled under 0.4%*D* to 0.6%*D* (*D* denotes the outer diameter of the segment ring) to prevent the operational distress. To be consistent with this code requirement, the limiting convergence deformation of the segment ring is taken as 0.6%*D* in this study.

Step 4: Repeating the performance analysis in Step 3 for all segment rings

In this step, the performance analysis of the segment ring presented in Step 3 is repeated for all segment rings of the shield tunnel, as shown with the inner loop in Figure 1. This in turn yields a series of factors of safety (with respect to either structural safety or serviceability), as different segment rings can exhibit different factors of safety due to the existence of the longitudinal variation of input parameters. Thus, the mean values of the factors of safety, denoted as μ_{Fs1} and μ_{Fs2}, are computed to represent the overall performance of the shield tunnel with respect to the structural safety and serviceability, respectively; whereas, the standard deviations of the factors of safety, denoted as σ_{Fs1} and σ_{Fs2}, are calculated to reflect the variation (or degree of uncertainty) of the performance of the shield tunnel with respect to the structural safety and serviceability, respectively.

Step 5: Repeating MCS runs to yield a converged solution of tunnel performance

Here, the performance analysis procedures of the shield tunnel presented in Step 1, Step 2, Step 3, and Step 4 are repeated for a specified number of MCS runs for purposes of deriving a converged solution of tunnel performance, as shown with the outer loop in Figure 1; since different MCS samples (of tunnel input parameters) could yield different sets of the mean (i.e.,

206 μ_{Fs1} and μ_{Fs2}) and standard deviation (i.e., σ_{Fs1} and σ_{Fs2}) of the tunnel performance. The
207 accuracy of MCS results depends on the number of MCS samples (Rubinstein and Kroese 2007;
208 Wang 2011), and the number of MCS samples required for different targets is quite different
209 (Wang 2013). In this paper, the convergence criterion of MCS results is determined as follows: if
210 the relative variation of MCS results caused by the increase of MCS samples is less than 1.0%,
211 then the convergence is achieved; otherwise, the convergence is not achieved and the number of
212 MCS samples is not sufficient. Note that the MCS results, in this paper, are referred to the
213 statistics of the mean and standard deviation of the tunnel performance (i.e., μ_{Fs1}, μ_{Fs2}, σ_{Fs1},
214 and σ_{Fs2}).
215
216 **Robust Design Methodology of Shield Tunnels**
217 The authors propose a new robustness measure for the robust design of shield tunnels that
218 enables an efficient consideration of the longitudinal variation of tunnel performance (due to the
219 existence of the longitudinal variation of input parameters). The formulation of the new
220 robustness measure and the complete multi-objective optimization setting of the robust design
221 methodology are presented below.
222 **New robustness measure for shield tunnels**
223 Robust design, which originated in the field of industrial engineering (Taguchi 1986;
224 Tsui 1992; Chen et al. 1996), aims to make the system response of a design robust against, or
225 insensitive to, the variation of hard-to-control noise factors by adjusting the easy-to-control
226 design parameters. Measuring the design robustness is an absolute necessity in a robust design. It
227 is noted that while various robustness measures have been reported in geotechnical engineering,
228 such as feasibility-based robustness measure (Juang et al. 2013; Wang et al. 2013), variation-

based robustness measure (Juang et al. 2014; Wang et al. 2014), signal-to-noise ratio-based robustness measure (Gong et al. 2014b; Gong et al. 2015b), and sensitivity-based robustness (Gong et al. 2014c), all these reported robustness measures are adopted for the analysis and design of a geotechnical system with only one or two system responses of concern, they are not valid for a geotechnical system with a large number of system responses of concern. The robust design of a tunnel longitudinal structure involves hundreds of system responses.

Given the longitudinal variation of tunnel input parameters (termed noise factors in the context of robust design), different segment rings might exhibit different system responses (i.e., Fs_1 and Fs_2). Thus, the reported robustness measures cannot be directly used for the robust design of a tunnel longitudinal structure. In fact, if the reported robustness measures are directly used for the robust design of the tunnel longitudinal structure, the design robustness evaluation of candidate designs could be computationally prohibitive and the screening of candidate designs could be a significant challenge. For example, for a tunnel longitudinal structure that consists of 300 segment rings, 600 robustness indexes need to be computed and optimized; since both the structural safety and the serviceability of each segment ring should be studied.

In this paper, the signal-to-noise ratio (*SNR*) of the factor of safety (Fs) is adapted for the robust design of the tunnel longitudinal structure (Gong et al. 2014b).

$$SNR = 10\log_{10}\left(\frac{\mu_{\mathrm{Fs}}{}^2}{\sigma_{\mathrm{Fs}}{}^2}\right) \tag{1}$$

where μ_{Fs} and σ_{Fs} are the mean and standard deviation of the factor of safety (with respect to the tunnel performance), respectively, which are readily computed using the procedure described in Step 4 in the previous section. Intuitively, a higher *SNR* value signals a lower variability of tunnel performance (i.e., Fs_1 and Fs_2) and, thusly, higher design robustness. Given the tunnel

input parameters along the longitudinal direction, the *SNR* of the tunnel performance is easily calculated, and then, the degree of the longitudinal variation of the tunnel performance, which arises from the longitudinal variation of input parameters, can be readily assessed.

As mentioned previously, different MCS samples, in terms tunnel input parameters (i.e., k_v, k_h, c, ϕ, H_W, and q_0) along the longitudinal direction, can result in different values of μ_{Fs} and σ_{Fs}. The variation in μ_{Fs} and σ_{Fs} creates further uncertainty in the computed *SNR*. Thus, a new robustness measure (R), which is based upon the statistics of *SNR*, is proposed herein to measure the design robustness of the tunnel longitudinal structure (against the longitudinal variation of input parameters):

$$R = \mu_{SNR} - 2\sigma_{SNR} \tag{2}$$

where μ_{SNR} and σ_{SNR} are the mean and standard deviation of *SNR* with respect to the tunnel performance, respectively, which are readily computed using the procedure described in Step 5 in the previous section.

As the robustness measure (R), defined in Eq. (2), is basically the same as *SNR*, greater design robustness is achieved with a greater R value. Here, the mean minus two standard deviations is adopted to approximate the lower end of *SNR*. We select the lower end of *SNR* as a robustness measure so as to achieve at least a certain level of *SNR* in the robust design optimization of a tunnel longitudinal structure. Furthermore, the robustness measure (R), defined in Eq. (2), enables an explicit consideration the variation of *SNR* among those obtained with different MCS samples. Note that MCS is used in this study to simulate the longitudinal variation of input parameters, as plotted in Figure 1; and thus, the robustness of the tunnel performance against the longitudinal variation of input parameters can be effectively captured with the formulated robustness measure.

Multi-objective optimization: design robustness versus cost efficiency

The goal of robust design is to derive an *optimal* design in the design space (**DS**), which is represented by a set of design parameters (***d***), such that the system response is robust against, or insensitive to, the variation of noise factors (***θ***) (Taguchi 1986; Tsui 1992; Chen et al. 1996). The desire to maximize the design robustness, however, must be balanced with the desire to minimize the cost, while satisfying the performance requirements (Liu et al. 2013; Juang et al. 2013&2014; Wang et al. 2013; Gong et al. 2014b&c; Khoshnevisan et al. 2014&2015). In other words, the robust design of the tunnel longitudinal structure can be implemented as a multi-objective optimization problem, as shown in Figure 4.

The optimization setting illustrated in Figure 4 depicts that the performance requirement (g) and design robustness (R) can be expressed as a function of design parameters (***d***) and noise factors (***θ***), while the cost (C) is determined with only the design parameters (***d***). Thus, the robust design can be realized through the adjustment of the design parameters (***d***).

Generally, the desire to maximize the design robustness and the desire to minimize the cost are two conflicting design objectives. As such, a single best design is unattainable in this optimization involving two conflicting design objectives (see Figure 4). Rather, the optimization tends to yield a set of non-dominated optimal designs (Deb et al. 2002; Juang et al. 2013). These non-dominated optimal designs collectively form a Pareto front that elucidates a tradeoff between design robustness and cost efficiency. The Pareto front can usually be obtained with algorithms such as the non-dominated sorting genetic algorithm version II (NSGA-II) (Deb et al. 2002); alternatively, the Pareto front can also be constructed using a series of single-objective optimization procedures (Khoshnevisan et al. 2015).

By presenting a tradeoff between design robustness and cost efficiency, the Pareto front can aid in making an informed design decision. For example, either the least cost design that is above a pre-specified level of design robustness (R_T) or the most robust design that falls within a pre-specified cost level (C_T) could be identified as the most preferred design in the design space. The selection of an optimal level of design robustness or cost, however, may be problem-specific and person-specific. Thus, when no design preference is specified by the owner or client, the knee point on the Pareto front, which represents the best compromise between design robustness and cost efficiency, may be taken as the most preferred design in the design space (Juang et al. 2014; Gong et al. 2014c; Gong et al. 2015b).

Design Example

To demonstrate the new framework for shield tunnel performance analysis and the proposed robust design methodology of shield tunnels, an illustrative example of the robust design of a shield tunnel with a longitudinal length of 300 m is presented. Note that while it is a hypothetical example, the input parameters are adapted from those of real-world tunnels in Shanghai, China.

Parameters setting in the illustrative example

In the robust design of the tunnel longitudinal structure, the input parameters are first classified into two categories: easy-to-control design parameters ($\boldsymbol{d}$) and hard-to-control noise factors ($\boldsymbol{\theta}$). Note that the design parameters are the input parameters that the designer may easily adjust: segment thickness (t), diameter of steel bolts (i.e., D_c and D_l for the circumferential bolts and longitudinal bolts, respectively) and steel reinforcement ratio of tunnel segment (ρ).

What the designer cannot easily adjust and characterize with certainty, however, are the noise factors ($\boldsymbol{\theta}$): vertical ground stiffness (k_v), horizontal ground stiffness (k_h), effective cohesion (c), effective friction angle (ϕ), ground water table (H_w) and ground surcharge (q_0). For illustration, the stationary random fields are used herein to model the longitudinal variation of noise factors; the statistics of these noise factors are listed in Table 1. In this case, the shield tunnel is assumed to be embedded in a homogeneous soil. It should be noted that the robust design methodology is applicable to layered deposits; however, multiple sets of input parameters would be required. To be more realistic, the mean and standard deviation of the noise factors listed in Table 1 are estimated based upon the available geological and geotechnical data described in Shanghai Foundation Design Code (1999). While it is acknowledged that different soil parameters may exhibit different scales of fluctuation in the horizontal direction, typically the value is in the range of 40-60 m (Phoon and Kulhawy 1999); in this paper, the scales of fluctuation of these noise factors are assumed to be 50 m. The data listed in Table 1 are typical values that are consistent with the input parameters used in Shanghai metro. For the design of a real-world shield tunnel at a locality, the statistical parameters should be characterized based on site exploration data, published literature, and local experience.

For ease of illustration, the unit weight of soil (γ_s), material parameters of the precast tunnel segment and steel (i.e., reinforcement of tunnel segment and bolts), and the geometries of the precast tunnel segment are assumed as constants, since the variability of each of these parameters is relatively low and negligible. The embedded depth (H), a vertical distance that is measured from the tunnel crown to the ground surface, is also assumed as a constant. The parameter settings are listed in Table 2. Note that the data listed in Table 2 are determined based upon the local experience in Shanghai.

Effectiveness of the new framework for shield tunnel performance analysis

With the statistics of the noise factors listed in Table 1, the performance of the example tunnel can be readily analyzed using our previously presented framework. Note that plotted in Figure 5 are the noise factors along the longitudinal direction that are generated with one MCS run. The great variance of the noise factors in the longitudinal domain makes determining the critical tunnel cross-sections of this shield tunnel most difficult. Here, the simplified 1-D FEM method, developed by the authors (Huang et al. 2015), is used to analyze the longitudinal behavior of this shield tunnel. The results of the 1-D FEM analysis, including tunnel settlement (w), longitudinal rotation (θ_L), longitudinal bending moment (M_L) and longitudinal shear force (Q_L), are plotted in Figure 6. As noted, a significant longitudinal variation of tunnel longitudinal behaviors is observed. The design parameters of this shield tunnel are: t = 0.35 m, ρ = 0.5%, D_c = 30 mm, and D_l = 30, which are comparable with the design parameters of typical Shanghai metro tunnels.

Figure 5 shows the generated noise factors along the longitudinal direction and Figure 6 shows the tunnel longitudinal behaviors. Based on these results, the performance (i.e., structural safety Fs_1 and serviceability Fs_2) of each segment ring of this shield tunnel can be analyzed using the aforementioned 2-D analytical model (Gong et al. 2015a). Figure 7 shows the resulted longitudinal variation of tunnel performance, in terms of Fs_1 (with respect to the structural safety of the segment ring) and Fs_2 (with respect to the serviceability of the segment ring). Note that different tunnel performances exhibit upon different segment rings of this shield tunnel, which are reflected by the longitudinal variation of the factors of safety (i.e., Fs_1 and Fs_2). Thus, the performance of this shield tunnel cannot be assessed with the results of a few segment rings, as is adopted in the conventional design practice.

Different MCS runs can generate different longitudinal variations of noise factors, which in turn results in an expected variance in the longitudinal variations of tunnel performance. For example, the longitudinal variation of tunnel performance plotted in Figure 7 is the analysis result of the longitudinal variation of noise factors plotted in Figure 5. Therefore, a series of MCS runs must be conducted to derive a converged solution of tunnel performance, in terms of the statistics of the mean and standard deviation of the tunnel performance (i.e., μ_{Fs1}, μ_{Fs2}, σ_{Fs1}, and σ_{Fs2}), as per Step 5 of the new analysis framework presented previously. Figures 8(a) and 8(b) show the computed values of the mean and standard deviation of the overall factors of safety with different number of MCS samples. It is noted that the converged solution of the mean and standard deviation of the overall factors of safety can be achieved with 500 MCS samples. Figures 8(c) and 8(d) further show the computed values of the mean and standard deviation of the signal-to-noise ratios (*SNR*) with different number of MCS samples. The converged solution of the mean and standard deviation of the *SNR* can also be achieved with 500 MCS samples. Therefore, the number of MCS samples in this study is set at 500 for sampling the longitudinal variation of noise factors.

It is noted that the overall factors of safety (in terms μ_{Fs1} and μ_{Fs2}) and *SNR* (in terms of SNR_1 and SNR_2) of this shield tunnel fit well with normal distributions, as depicted in Figure 9. As demonstrated in Figures 9(a) and 9(b), the variations of the overall factors of safety are relatively small and may be neglected. For example, the means of μ_{Fs1} and μ_{Fs2} are 1.39 and 2.49, respectively, while the standard variations of μ_{Fs1} and μ_{Fs2} are 0.07 and 0.11, respectively. The variations of the computed *SNR*, as shown in Figure 9(c) and 9(d), are quite significant however, and cannot be ignored. Specifically, the means of SNR_1 and SNR_2 are 10.33 and 4.63, respectively, while the standard variations of SNR_1 and SNR_2 are 0.77 and 1.12, respectively.

Therefore, the means of μ_{Fs1} and μ_{Fs2} are used in this study to assess the performance requirements of the candidate design of the shield tunnel; and, the design robustness of the candidate design is measured with proposed robustness measure (R) in Eq. (2). Figures 9(c) and 9(d) also show the computed design robustness, in terms of R_1 and R_2, of this shield tunnel.

Finally, the failure probabilities with respect to both the structural safety and the serviceability of the segment ring of this longitudinal shield tunnel are computed using the new analysis framework presented previously. For this shield tunnel, the failure probabilities for structural safety and serviceability are 2.14×10^{-1} and 2.98×10^{-2}, respectively, based on 2,000 MCS samples (see Figures 10a and 10b). These predicted failure probabilities are much greater than the typically acceptable failure probability of 10^{-3} to 10^{-4}, suggesting high likelihood of tunnel performance problems. This result is consistent with the long term structural health monitoring of the existing shield tunnels in Shanghai, which revealed that a great proportion of the segment rings suffered performance problems such as segment crack, joint opening, and water leakage. As a comparison, the failure probabilities of the segment ring of this shield tunnel computed with the conventional tunnel analysis method (e.g., Lee et al. 2001), in which the longitudinal variation of input parameters cannot be considered, are significantly lower, i.e. 4.0×10^{-5} and 0, respectively (see Figures 11a and 11b). These probabilities are much less than the typically acceptable failure probability of 10^{-3} to 10^{-4}, suggesting very low likelihood of tunnel performance problems. Thus, the results obtained with the conventional tunnel analysis method are not consistent with the long term field observations.

In summary, a consideration of the longitudinal variation of input parameters adds more realism for the prediction of the performance of the longitudinal shield tunnels. This adds significance to the proposed framework for shield tunnel performance analysis.

Effect of design parameters on tunnel performance and design robustness

In reference to the robust design optimization setting in Figure 4, the tunnel performance and design robustness are expressed as a function of design parameters (***d***) and noise factors (***θ***). Thus, a series of parametric analyses are necessary to investigate how an adjustment of design parameters (***d***) affects both the tunnel performance, in terms of the means of μ_{Fs1} and μ_{Fs2}, and the design robustness, in terms of R_1 and R_2. This series of parametric studies, the results of which are shown in Figures 12 and 13, provides a basis for the robust design of the shield tunnel.

As shown in Figure 12(a), the tunnel performance with respect to both the structural safety and the serviceability (in terms of the means of μ_{Fs1} and μ_{Fs2}, respectively) increases with the increase of the segment thickness. The shield tunnel structure with a larger segment thickness can, naturally, bear more internal forces and yield less convergence deformation. As indicated in Figure 12(b), as the bolt diameter of the circumferential joints increases, the tunnel performance with respect to the structural safety decreases significantly, whereas the tunnel performance with respect to the serviceability increases linearly. The plots in Figure 12(b) indicate that the shield tunnel structure with a larger bolt diameter of the circumferential joints yields larger internal forces and less convergence deformation. In Figure 12(c), as the bolt diameter of the longitudinal joints increases, the tunnel performance with respect to the structural safety improves, while the tunnel performance with respect to the serviceability improves initially and then begins to degrade. The variation of the tunnel performance due to the adjustment of the diameter of the longitudinal joints is not distinct, however. Although the steel reinforcement ratio of the tunnel segment can enhance the bearing capacity of the tunnel ring, it has very little effect on the circumferential stiffness of the segment ring. Thus, the tunnel performance with respect to the structural safety improves significantly with the increase of the

steel reinforcement ratio of tunnel segment, while the tunnel performance with respect to the serviceability is hardly affected by the adjustment of the reinforcement ratio of tunnel segment, as depicted in Figure 12(d).

Figure 13 shows the effect of design parameters on the design robustness of the shield tunnel. As shown in Figure 13(a), although an increase of the segment thickness enhances the design robustness of the shield tunnel with respect to the structural safety (indicated by the increase of R_1), the design robustness with respect to the serviceability is degraded (indicated by the decrease of R_2). The effect of the increase of the segment thickness on the design robustness becomes less significant as the segment thickness grows. As shown in Figure 13(b), the increase of the bolt diameter of the circumferential joints always leads to the decrease of design robustness with respect to the serviceability, whereas the design robustness with respect to the structural safety increases initially and then begins to decrease. Similarly, the increase of the bolt diameter of the longitudinal joints enhances the design robustness with respect to the serviceability, whereas the design robustness with respect to the structural safety increases initially and then begins to decrease, as depicted in Figure 13(c). Finally, in Figure 14(d), the increase of the steel reinforcement ratio of tunnel segment enhances the design robustness with respect to the structural safety, but has little effect on the design robustness with respect to the serviceability.

The results of these parametric analyses, shown in Figures 12 and 13, offer an insight on the effects of the easy-to-control design parameters on the performance and design robustness of the longitudinal shield tunnel. They provide a basis for the robust design of shield tunnels: the robust design of shield tunnels can indeed be achieved by a careful adjustment of design parameters, which is the essence of robust design.

Robust design results

For illustration purposes, a discrete design space (**DS**) is adopted in this study. With the ranges of design parameters tabulated in Table 3, this design space consists of 500 discrete candidate designs. Of course, a continuous design space may be adopted if so desired based on local experience in a real-world application. For the performance requirements (i.e., structural safety and serviceability of segment rings) of the shield tunnel, the target factors of safety with respect to both the structural safety and the serviceability are set at 1.5. In other words, the performance requirements of this shield tunnel design problem consist of two conditions: the mean of $\mu_{Fs1} > 1.5$ and the mean of $\mu_{Fs2} > 1.5$. As outlined in Figure 4, the cost of the shield tunnel is also a design objective to be optimized in the robust design optimization. For illustration purpose, only the material cost of the shield tunnel is considered, which consists of the segment concrete cost, steel reinforcement cost, and joint bolts cost. According to Gong et al. (2014b), the unit prices of the concrete segment, reinforcement steel, and joint bolts in a typical Shanghai metro tunnel are c_c = 600 RMB/m^3 (97.77 USD/m^3), c_s = 4000 RMB/10^{3}kg (645.16 USD/10^{3}kg), and c_b = 10 RMB/kg (1.61 USD/kg), respectively. Thus, the cost function in the robust design of the shield tunnel, denoted as $C(\boldsymbol{d})$ in Figure 4, is computed as follows:

$$C(\boldsymbol{d}) = c_c Q_c + c_s Q_s + c_b Q_b \quad (3)$$

where Q_c, Q_s, and Q_b are the quantity of concrete segment (m^3), reinforcement steel (10^3 kg), and joint bolts (kg) of the shield tunnel longitudinal structure, respectively. It is noted that while the above cost-estimation model is considered adequate, other more sophisticated models can also be adopted. Although the design results may be affected by the cost-estimation model (Wang and Kulhawy 2008), this is not the limitation of the robust design methodology; rather, the estimation of cost is part of any design process. This issue is beyond the scope of this paper.

Once the performance requirements (i.e., structural safety and serviceability of segment rings), the cost, and the design robustness of each candidate design in the design space are assessed, the robust design optimization is then performed. It is noted that the robust design optimization yields a series of non-dominated optimal designs, as plotted in Figure 14, rather than a single best design. Note again the evident conflict of reconciling the desire to maximize the design robustness and the desire to minimize the cost. The obtained non-dominated optimal designs collectively form a 3-D Pareto front, since there are three objectives involved in this optimization (i.e., design robustness with respect to the structural safety R_1, design robustness with respect to the serviceability R_2, and cost efficiency C).

In a design decision involving a tradeoff between design robustness and cost efficiency, the determination of an appropriate level of design robustness or cost might be problem-specific and person-specific. If no design preference is specified by the owner or client, the knee point on the Pareto front may be taken as the most preferred design (Juang et al. 2014; Gong et al. 2014c; Gong et al. 2015b). Here, the marginal utility function-based approach (Branke et al. 2004; Gong et al. 2014c; Gong et al. 2015b) is employed to locate the knee point on the Pareto front. The identified knee point is also plotted in Figure 14. Note that on the upper side of the knee point, a slight improvement in the design robustness would significantly increase the cost; on the other side of the knee point, however a slight reduction in cost would require a huge sacrifice in the design robustness.

Also plotted in Figure 14 is the actual design (or real-world design) adopted in Shanghai metro tunnels. It is noted that greater design robustness (indicated by a larger R) and greater cost efficiency (indicated by a lower C) can be achieved with the knee point obtained with the robust design optimization, compared to the actual design in Shanghai. A detailed comparison of these

two designs is provided in Table 4. One of the features compared here is the feasibility, denoted as f, which is the likelihood that the shield tunnel will meet the requirements of tunnel performance (i.e., structural safety and serviceability of segment rings). This feasibility is defined as follows:

$$f_1 = \Pr\left[\mathrm{Fs}_1 > 1.0\right] \tag{4a}$$

$$f_2 = \Pr\left[\mathrm{Fs}_2 > 1.0\right] \tag{4b}$$

where f_1 and f_2 are the feasibilities with respect to the structural safety and serviceability of the shield tunnel, respectively; and Pr[Fs > 1.0] represents the conditional probability that the factor of safety (Fs) is greater than 1.0 in the face of the unforeseen longitudinal variation of noise factors. Indeed, the feasibility defined in Eq. (4) may also be interpreted as the percentage of segment rings that meet the tunnel performance requirement (i.e., Fs > 1.0).

Compared to the actual design in Shanghai, the bolt diameter of the circumferential joints (D_c) of the knee point, obtained with the robust design optimization, is reduced from 30 mm to 20 mm. As a result, the design feasibility with respect to the structural safety (f_1), tunnel performance with respect to the structural safety (in terms of the mean of μ_{Fs1}), cost efficiency (C), and design robustness with respect to both the structural safety (R_1) and the serviceability (R_2) are significantly improved. For example, the feasibility with respect to the structural safety is increased from 0.7846 to 0.9607 and the design robustness with respect to the serviceability is increased from 2.31 to 4.89. However, the design feasibility and tunnel performance with respect to the serviceability (i.e., f_2 and the mean of μ_{Fs2}) are degraded somewhat, although the tunnel performance requirements are still satisfied.

It should be noted that the most preferred design in the design space (i.e., knee point on the Pareto front) may vary with the robust design optimization settings (e.g., cost-estimation

model, design space, and target factors of safety). Here, the robust design optimization of this illustrative shield tunnel is reanalyzed and redesigned with different target factors of safety with respect to the tunnel performance, and the robust design results are listed in Table 5. The results show that different robust design optimization settings can produce different final designs of the shield tunnel. For a given cost-estimation model and design space, as the target factor of safety (with respect to the tunnel performance) increases, the design feasibility (i.e., f_1 and f_2), tunnel performance (i.e., the means of μ_{Fs1} and μ_{Fs2}), and cost (C) of the most preferred designs tend to increase, while the number of the non-dominated optimal designs tends to decrease.

Conclusions

The authors present an improved design methodology for shield tunnels by carefully combining the robust geotechnical design methodology with the advanced framework for shield tunnel performance analysis. In the context of the proposed design methodology, the input parameters that are associated with the longitudinal variation (or spatial variation in the longitudinal domain) are classified as noise factors, while the input parameters that can be adjusted by the designer are classified as design parameters. The goal of the improved design methodology is then to identify an optimal design that is optimized with respect to the design robustness (against the longitudinal variation of noise factors) and cost efficiency, while satisfying the performance requirements. Based upon the presented results, the following conclusions are reached.

1) The proposed framework for shield tunnel performance analysis is shown capable of analyzing the longitudinal variation of input parameters (e.g., soil parameters, ground water table, and overburden). The proposed framework yields results (e.g., probabilities

of unsatisfactory performance of the segment ring) that are more consistent with the data from the structural health monitoring in Shanghai metro tunnels, compared to the conventional methods that cannot consider the longitudinal variation of input parameters. Nevertheless, further validation of the proposed framework against 3-D FEM solutions or field data would be valuable.

2) The modified robust design methodology for shield tunnels is capable of producing a robust shield tunnel design that is both cost efficient and robust against the longitudinal variation of noise factors, while meeting the requirements for tunnel performance (i.e., structural safety and serviceability of segment rings). Compared to the actual design in Shanghai, the most preferred design in the design space (i.e., knee point on the Pareto front) obtained with the robust design optimization exhibits greater design robustness, greater cost efficiency, and greater feasibility of tunnel performance.

3) Unlike the current design practices, the proposed robust design methodology considers the design robustness, cost efficiency, and tunnel performance requirements explicitly and simultaneously. Utilizing the multi-objective optimization, the proposed robust design methodology yields a Pareto front that shows a trade-off relationship between design robustness and cost efficiency. The Pareto front with or without the identified knee point can aid in selecting the most preferred design.

4) Apart from the multi-objective optimization, a new robustness measure, which is based upon the signal-to-noise ratio (*SNR*), is proposed for the shield tunnel performance analysis. The new robustness measure is adapted specifically for considering the longitudinal variation of tunnel performance (due to the existence of the longitudinal

variation of noise factors), and is demonstrated effective for use with the proposed robust design of shield tunnels.

5) Parametric analyses show that the segment thickness, bolt diameter of the circumferential joints, and bolt diameter of the longitudinal joints are the key design parameters that affect the tunnel performance and design robustness with respect to both the structural safety and the serviceability. While the steel reinforcement ratio of tunnel segment significantly affects the tunnel performance and design robustness with respect to the structural safety, it does not significantly affect tunnel performance and design robustness with respect to the serviceability of the segment.

ACKNOWLEDGMENTS

This material is based upon research partially supported by the National Science Foundation under Grant Number CMMI-1200117 (Project titled "*Transforming Robust Design Concept into a Novel Geotechnical Design Tool*"; Richard Fragaszy was the Program Director at NSF and Hsein Juang of Clemson University was the Principal Investigator). Any opinions, findings, and conclusions or recommendations expressed in this material are those of the authors and do not necessarily reflect the views of the National Science Foundation. The first author wishes to acknowledge the financial support by NSF and the Glenn Department of Civil Engineering, Clemson University through the Aniket Shrikhande Graduate Fellowship. The last author wishes to acknowledge the financial support provided by NSF through its East Asia and Pacific Summer Institute (EAPSI) program (Grant Number 1414635) for his summer research at Tongji University, China.

References

American Transportation Research Board (ATRB). 2000. Design and Construction of Transportation Facilities.

Baker, R. 1984. Modeling soil variability as a random field. Journal of the International Association for Mathematical Geology, 16(5): 435-448.

Bobet, A. 2001. Analytical solutions for shallow tunnels in saturated ground. Journal of Engineering Mechanics, 127(12): 1258-1266.

Branke, J., Deb, K., Dierolf, H., and Osswald, M. 2004. Finding knees in multiobjective optimization. In Parallel problem solving from nature - PPSN VIII. pp. 722-731.

Cao, Z.J. and Wang, Y. 2014. Bayesian model comparison and characterization of undrained shear strength. Journal of Geotechnical and Geoenvironmental Engineering, 140(6): 04014018.

Chen, W., Allen, J.K., Tsui, K.L., and Mistree, F. 1996. A procedure for robust design: minimizing variations caused by noise factors and control factors. Journal of Mechanical Design, 118(4): 478-485.

Cho, S.E. 2007. Effects of spatial variability of soil properties on slope stability. Engineering Geology, 92(3): 97-109.

Deb, K., Pratap, A., Agarwal, S., and Meyarivan, T. 2002. A fast and elitist multi-objective genetic algorithm: NSGA-II. IEEE Transactions on Evolutionary Computation, 6(2): 182-197.

Fenton, G.A. 1999. Estimation for stochastic soil models. Journal of Geotechnical and Geoenvironmental Engineering, 125(6): 470-485.

616 Fenton, G.A, and Griffiths, D.V. 2002. Probabilistic foundation settlement on spatially random
617 soil. Journal of Geotechnical and Geoenvironmental Engineering, 128(5): 381-390.
618 Fenton, G.A., and Griffiths, D.V. 2003. Bearing-capacity prediction of spatially random c φ soils.
619 Canadian Geotechnical Journal, 40(1): 54-65.
620 Gong, W., Luo, Z., Juang, C.H., Huang, H., Zhang, J., and Wang, L. 2014a. Optimization of site
621 exploration program for improved prediction of tunneling-induced ground settlement in
622 clays. Computers and Geotechnics, 56: 69-79.
623 Gong, W., Wang, L., Juang, C.H., Zhang, J., and Huang, H. 2014b. Robust geotechnical design
624 of shield-driven tunnels. Computers and Geotechnics, 56: 191-201.
625 Gong, W., Khoshnevisan, S., and Juang, C.H. 2014c. Gradient-based design robustness measure
626 for robust geotechnical design. Canadian Geotechnical Journal, 51: 1331-1342.
627 Gong, W., Juang, C.H., Huang, H., Zhang, J., and Luo, Z. 2015a. Improved analytical model for
628 circumferential behavior of jointed shield tunnels considering the longitudinal differential
629 settlement. Tunnelling and Underground Space Technology, 45, 153-165.
630 Gong, W., Wang, L., Khoshnevisan, S., Juang, C.H., Huang, H., and Zhang, J. 2015b. Robust
631 geotechnical design of earth slopes using fuzzy sets. Journal of Geotechnical and
632 Geoenvironmental Engineering, 141(1): 04014084.
633 Horvath, J.S. 1983. Modulus of subgrade reaction: new perspective. Journal of Geotechnical
634 Engineering, 109(12): 1591-1596.
635 Huang, H., Gong, W., Khoshnevisan, S., Juang, C.H, Zhang, D., and Wang, L. 2015. Simplified
636 procedure for finite element analysis of the longitudinal performance of shield tunnels
637 considering spatial soil variability in longitudinal direction. Computers and Geotechnics, 64:
638 132-145.

639 Huang, X., Huang, H.W., and Zhang, J. 2012. Flattening of jointed shield-driven tunnel induced
640 by longitudinal differential settlements. Tunnelling and Underground Space Technology, 31:
641 20-32.
642 International Tunnelling Association (ITA). 2000. Guidelines for the design of shield tunnel
643 lining. Tunnelling and Underground Space Technology, 15(3): 303-331.
644 Juang, C. H., Wang, L., Hsieh, H. S., and Atamturktur, S. 2014. Robust geotechnical design of
645 braced excavations in clays. Structural Safety, 49: 37-44.
646 Juang, C.H., Wang, L., Liu, Z., Ravichandran, N., Huang, H., and Zhang, J. 2013. Robust
647 geotechnical design of drilled shafts in sand: New design perspective. Journal of
648 Geotechnical and Geoenvironmental Engineering, 139(12): 2007-2019.
649 Khoshnevisan, S., Gong, W., Juang, C.H., and Atamturktur, S. 2015. Efficient robust
650 geotechnical design of drilled shafts in clay using a spreadsheet. Journal of Geotechnical
651 and Geoenvironmental Engineering, 141(2): 04014092.
652 Khoshnevisan, S., Gong, W., Wang, L., and Juang, C.H. 2014. Robust design in geotechnical
653 engineering – An update. Georisk: Assessment and Management of Risk for Engineered
654 Systems and Geohazards, 8(4): 217-234.
655 Koyama Y. 2003. Present status and technology of shield tunneling method in Japan. Tunneling
656 and Underground Space Technology, 18(2-3): 145-159.
657 Lee, K.M., and Ge, X.W. 2001. The equivalence of a jointed shield-driven tunnel lining to a
658 continuous ring structure. Canadian Geotechnical Journal, 38(3): 461-483.
659 Lee, K.M., Hou, X.Y., Ge, X.W., and Tang, Y. 2001. An analytical solution for a jointed
660 shield‐driven tunnel lining. International Journal for Numerical and Analytical Methods in
661 Geomechanics, 25(4): 365-390.

662 Liao, S.M., Hou, X.Y., and Peng, F.L. 2005. Longitudinal shear transfer of tunnel and its 1D
663 analytical solution. Chinese Journal of Rock Mechanics and Engineering, 24(7): 1110-1116
664 (in Chinese).
665 Liao, S.M., Peng, F.L., and Shen, S.L. 2008. Analysis of shearing effect on tunnel induced by
666 load transfer along longitudinal direction. Tunnelling and Underground Space Technology,
667 23(4): 421-430.
668 Lin, P.S., Yang, L.W., and Juang, C.H. 1998. Subgrade reaction and load-settlement
669 characteristics of gravelly cobble deposits by plate-load tests. Canadian Geotechnical
670 Journal, 35(5): 801-810.
671 Liu, Z., Atamturktur, S., and Juang, C.H. 2013. Performance based robust design optimization of
672 steel moment resisting frames. Journal of Constructional Steel Research, 89: 165-174.
673 Liu, Z., Atamturktur, S., and Juang, C.H. 2014. Reliability based multi-objective robust design
674 optimization of steel moment resisting frame considering spatial variability of connection
675 parameters. Engineering Structures, 76: 393-403. DOI: 10.1016/j.engstruct.2014.07.024.
676 Luo, Z., Atamturktur, S., Cai, Y., and Juang, C.H. 2012. Reliability analysis of basal-heave in a
677 braced excavation in a 2-D random field. Computers and Geotechnics, 39: 27-37.
678 Ministry of Construction of the People's Republic of China (MCPRC). 2003. Code for Design of
679 Metro (GB50157-2003). Beijing, China Building Industry Press (in Chinese).
680 Phoon, K.K. and Kulhawy, F.H. 1999. Characterization of geotechnical variability. Canadian
681 Geotechnical Journal, 36(4): 612-624.
682 Rubinstein, R.Y., and Kroese, D.P. 2007. Simulation and the Monte Carlo method (2dn edition).
683 John Wiley & Sons, NY.

Sadrekarimi, J., and Akbarzad, M. 2009. Comparative study of methods of determination of coefficient of subgrade reaction. Electronic Journal of Geotechnical Engineering, 14: 1-14.

Shanghai Municipal Construction Committee. 1999. Foundation Design Code (DGJ08-11-1999). Shanghai (in Chinese).

Taguchi, G. 1986. Introduction to Quality Engineering: Designing Quality into Products and Processes, Quality Resources, White Plains, NY.

Tsui, K.L. 1992. An overview of Taguchi method and newly developed statistical methods on robust design. IIE Trans., 24(5): 44-57.

Wang, L., Hwang, J. H., Juang, C. H., and Atamturktur, S. 2013. Reliability-based design of rock slopes – A new perspective on design robustness. Engineering Geology, 154, 56-63.

Wang, L., Juang, C.H., Atamturktur, S., Gong, W., Khoshnevisan, K. and Hsieh, H.S. 2014. Optimization of design of supported excavations in multi-layer strata. Journal of GeoEngineering, 9(1), 1-12.

Wang, Y. 2011. Reliability-based design of spread foundations by Monte Carlo Simulations. Geotechnique, 61(8): 677-685.

Wang, Y. (2013). MCS-based probabilistic design of embedded sheet pile walls. Georisk: Assessment and Management of Risk for Engineered Systems and Geohazards, 7(3): 151-162.

Wang, Y. and Cao, Z.J. 2013. Probabilistic characterization of Young's modulus of soil using equivalent samples. Engineering Geology, 159: 106-118.

Wang, Y. and Kulhawy, F.H. 2008. Economic design optimization of foundations. Journal of Geotechnical and Geoenvironmental Engineering, 134(8): 1097-1105.

Winkler, E. 1867. Die lehre von der elastizitat und fesigkeit [Dissertation]. Prague.

707 Wood, A.M.M. 1975. The circular tunnel in elastic ground. Géotechnique, 25(1): 115-127

708

Appendix A: Random field model of the longitudinal variation of input parameters

The stationary lognormal random field is used herein to model the longitudinal variation of input parameters of concern (θ). Given the statistical statistics of the tunnel input parameter (i.e., the mean μ, standard deviation σ, and the scale of fluctuation r), the tunnel input parameter, denoted as θ_{x_i}, at a specific longitudinal coordinate of x_i can be generated as follows (Gong et al. 2014a):

$$\theta_{x_i} = \exp\left[\mu_{\mathrm{n}} + \sigma_{\mathrm{n}} \cdot G_{\mathrm{n}}(x_i)\right] \tag{A1}$$

where μ_{n} and σ_{n} are the mean and standard deviation of $\ln(\theta)$, respectively, which are computed from the mean (μ_l) and standard deviation (σ_l) of the averaged tunnel input parameter (within the tunnel element domain) through the following transformations:

$$\sigma_{\mathrm{n}} = \sqrt{\ln\left[1+(\sigma_l/\mu_l)^2\right]} \tag{A2}$$

$$\mu_{\mathrm{n}} = \ln \mu_l - \frac{1}{2}\sigma_{\mathrm{n}}^2 \tag{A3}$$

The term G_{n} in Eq. (A1) represents a set of standard normal random variables with the autocorrelation function of $\rho(\theta_{x_i},\theta_{x_j})$ that is formulated in Eq. (A6). This set of standard normal random variables can be easily generated using Monte Carlo simulation (MCS).

In general, the mean of the averaged tunnel input parameter within the element domain (μ_l) is expected to be equal to the mean of the point tunnel input parameter at element nodes (μ). The variance of the averaged tunnel input parameter, however, is less than the variance of the point property when the local averaging effect is taken into account. For simplicity, the variance of the averaged tunnel input parameter within the element domain is computed as follows (Cho 2007):

$$\sigma_l^2 = \gamma(l)\sigma^2 \tag{A4}$$

where l is the length of the tunnel element of concern, and $\gamma(l)$ is a variance reduction factor bounded by 0 and 1.0 and computed as (Cho 2007):

$$\gamma(l) = \frac{1}{2}\left(\frac{r}{l}\right)^2\left[\frac{2l}{r} - 1 + \exp\left(-\frac{2l}{r}\right)\right] \quad \text{(A5)}$$

Further, the correlation between the averaged tunnel input parameters within different tunnel elements, in terms of θ_{x_i} (for element i) and θ_{x_j} (for element j), is computed by averaging the correlation between the tunnel input parameters at all points within the element lengths (Cho 2007):

$$\rho(\theta_{x_i}, \theta_{x_j}) = \frac{1}{l_i l_j}\int_{x_i-\frac{l_i}{2}}^{x_i+\frac{l_i}{2}}\int_{x_j-\frac{l_j}{2}}^{x_j+\frac{l_j}{2}} \rho(x_2 - x_1)\, d_{x_2} d_{x_1} \quad \text{(A6)}$$

where l_i and l_j are the longitudinal lengths of the element i and the element j, respectively; and $\rho(x)$ is the autocorrelation function among the point tunnel input parameters. Oftentimes, it is difficult to obtain a closed form solution of Eq. (A6). Alternatively, a numerical integration scheme such as the three-point Gauss numerical integration may be employed. In this study, the anisotropic exponential autocorrelation function is used to represent the autocorrelation among the point tunnel input parameters:

$$\rho(x) = \exp\left(-\frac{2|x|}{r}\right) \quad \text{(A7)}$$

where $|x|$ is the relative longitudinal distance of any two points of concern.

Appendix B: 1-D FEM solution of tunnel longitudinal behavior

For a tunnel longitudinal structure that is subject to the longitudinal variation of input parameters, specifically the vertical ground stiffness (k_v) of the ground under the tunnel and the overburden (q) on the tunnel, as shown in Figure 2, the longitudinal behavior of which, including tunnel settlement, longitudinal rotation, longitudinal bending moment, and longitudinal shear force can be studied using the 1-D FEM solution that based upon the Winkler elastic foundation theory (Huang et al. 2015). In the context of which, the element equilibrium equation is expressed as:

$$[\mathbf{K}]^{\mathrm{e}} \cdot [\boldsymbol{a}]^{\mathrm{e}} = [\mathbf{F}]^{\mathrm{e}} \tag{B1}$$

where $[\mathbf{K}]^{\mathrm{e}}$ is the local stiffness matrix of the tunnel element of concern; $[\boldsymbol{a}]^{\mathrm{e}}$ is the deformation vector of the element; and $[\mathbf{F}]^{\mathrm{e}}$ is the load vector of the element. The term $[\boldsymbol{a}]^{\mathrm{e}}$ in Eq. (B1) is expressed as:

$$[\boldsymbol{a}]^{\mathrm{e}} = \begin{bmatrix} \omega_1 & \theta_{\mathrm{L}1} & \omega_2 & \theta_{\mathrm{L}2} \end{bmatrix}^{\mathrm{T}}, \text{ in which } \theta_{\mathrm{L}i} = \left(\frac{dw}{dx} \right)_{x=x_i} \quad (i = 1 \text{ and } 2) \tag{B2}$$

where w_1 and w_2 are the settlements at the left end (referred to node i in Figure 2) and the right end (referred to node i+1 in Figure 2) of the element of concern (referred to element i in Figure 2), respectively; and, θ_1 and θ_2 are the longitudinal rotations at the left end and the right end of the element, respectively. The term $[\mathbf{K}]^{\mathrm{e}}$ in Eq. (B1) is constructed as:

$$[\mathbf{K}]^{\mathrm{e}} = [\mathbf{KB}]^{\mathrm{e}} + [\mathbf{KG}]^{\mathrm{e}} \tag{B3}$$

$$[\mathbf{KB}]^{\mathrm{e}} = \frac{\zeta E_{\mathrm{c}} I}{l^3} \begin{bmatrix} 12 & 6l & -12 & 6l \\ 6l & 4l^2 & -6l & 2l^2 \\ -12 & -6l & 12 & -6l \\ 6l & 2l^2 & -6l & 4l^2 \end{bmatrix} \tag{B4}$$

767 $$[\mathbf{KG}]^{e} = Dl\begin{bmatrix} \frac{13}{35}k_{v1}+\frac{3}{35}(k_{v2}-k_{v1}) & \frac{11}{210}k_{v1}l+\frac{1}{60}(k_{v2}-k_{v1})l & \frac{9}{70}k_{v1}+\frac{9}{140}(k_{v2}-k_{v1}) & -\frac{13}{420}k_{v1}l-\frac{1}{70}(k_{v2}-k_{v1})l \\ \frac{11}{210}k_{v1}l+\frac{1}{60}(k_{v2}-k_{v1})l & \frac{1}{105}k_{v1}l^2+\frac{1}{280}(k_{v2}-k_{v1})l^2 & \frac{13}{420}k_{v1}l+\frac{1}{60}(k_{v2}-k_{v1})l & -\frac{1}{140}k_{v1}l^2-\frac{1}{280}(k_{v2}-k_{v1})l^2 \\ \frac{9}{70}k_{v1}+\frac{9}{140}(k_{v2}-k_{v1}) & \frac{13}{420}k_{v1}l+\frac{1}{60}(k_{v2}-k_{v1})l & \frac{13}{35}k_{v1}+\frac{2}{7}(k_{v2}-k_{v1}) & -\frac{11}{210}k_{v1}l-\frac{1}{28}(k_{v2}-k_{v1})l \\ -\frac{13}{420}k_{v1}l-\frac{1}{70}(k_{v2}-k_{v1})l & -\frac{1}{140}k_{v1}l^2-\frac{1}{280}(k_{v2}-k_{v1})l^2 & -\frac{11}{210}k_{v1}l-\frac{1}{28}(k_{v2}-k_{v1})l & \frac{1}{105}k_{v1}l^2+\frac{1}{168}(k_{v2}-k_{v1})l^2 \end{bmatrix}$$

768 (B5)

769 where $[\mathbf{KB}]^{e}$ and $[\mathbf{KG}]^{e}$ are the local stiffness matrices of the element that arise from the elastic
770 beam and the ground under the tunnel, respectively; $\zeta E_c I$ is the equivalent flexural stiffness of
771 the tunnel longitudinal structure, which is computed as $\zeta E_c I = \frac{\pi}{64}\zeta E_c\left[D^4-(D-2t)^4\right]$; ζ is the
772 reduction factor of tunnel longitudinal flexural stiffness, the derivation of which can be found in
773 Liao et al. (2008); E_c is the elastic modulus of tunnel segment; D is diameter of the shield tunnel;
774 t is the thickness of tunnel segment; and, k_{v1} and k_{v2} are the subgrade reaction coefficients at the
775 left end and the right end of the element, respectively. The term $[\mathbf{F}]^{e}$ in Eq. (B1) is computed as:

776 $$[\mathbf{F}]^{e} = Dl\begin{bmatrix} \frac{1}{2}q_1+\frac{3}{20}(q_2-q_1) \\ \frac{1}{12}q_1l+\frac{1}{30}(q_2-q_1)l \\ \frac{1}{2}q_1+\frac{7}{12}(q_2-q_1) \\ -\frac{1}{12}q_1l-\frac{1}{20}(q_2-q_1)l \end{bmatrix} \quad \text{(B6)}$$

777 where q_1 and q_2 are the pressure loads at the left end and the right end of the element,
778 respectively.

779 Based on the element equilibrium equation developed in Eq. (B1), the global equilibrium
780 equation of the whole tunnel longitudinal structure can be assembled accordingly. As such, the
781 tunnel longitudinal deformation, including tunnel settlement (w) and longitudinal rotation (θ_L),
782 can be readily solved. Further, the longitudinal bending moment (M_L) and longitudinal shear

783 force (Q_L) of the shield tunnel can be computed. For example, the longitudinal internal forces at

784 node i and node (i+1), in terms of Q_{Li}, M_{Li}, $Q_{L(i+1)}$, and $M_{L(i+1)}$, are calculated as :

785 $$\begin{bmatrix} -Q_{Li} & M_{Li} & Q_{L(i+1)} & -M_{L(i+1)} \end{bmatrix}^{T} = [\mathbf{KB}]^{(i)} \cdot [\boldsymbol{a}]^{(i)} \quad \text{(B7)}$$

786 where $[\mathbf{KB}]^{(i)}$ is the local stiffness matrix of element i that arises from the elastic beam (see Eq.

787 B4); and $[\boldsymbol{a}]^{(i)}$ is the nodal deformation of element i, expressed as:

788 $$[\boldsymbol{a}]^{(i)} = \begin{bmatrix} \omega_i & \theta_{Li} & \omega_{i+1} & \theta_{L(i+1)} \end{bmatrix}^{T} \quad \text{(B8)}$$

789

Appendix C: Load condition for the performance analysis of segment rings

In reference to Figure 3, the load condition of the segment ring is defined as:

(1) Total vertical earth pressure at tunnel crown, p_1:

$$p_1 = q_0 + q_1 + q_2 \tag{C1}$$

where q_0 is the ground surcharge; and q_1 is the total earth pressure generated at tunnel crown, which is equal to the overburden earth pressure for the shallow tunnel:

$$q_1 = \sum_{i=1}^{n_s} \gamma_{si} h_i \tag{C2}$$

where γ_{si} is the total unit weight of soil layer i; h_i is the thickness of soil layer i; n_s is the total number of soil layers above tunnel crown; and q_2 is the total earth pressure developed in the shoulder region of tunnel, estimated as:

$$q_2 = \left(1 - \frac{\pi}{4}\right) R \gamma_{as} \tag{C3}$$

where R is the calculating radius of the shield tunnel, defined as the average of outer radius and inner radius; and γ_{as} is the averaged total unit weight of the soil layers in the shoulder region.

(2) Reaction pressure at the tunnel bottom, p_2, which equals to the summation of p_1 and self-weight of tunnel lining is:

$$p_2 = p_1 + \pi t \gamma_c \tag{C4}$$

where t is the thickness of tunnel segment; and γ_c is the unit weight of tunnel segment.

(3) To determine the total lateral earth pressure at tunnel crown, p_3, Rankine active earth pressure is employed:

$$p_3 = q_1' \tan^2\left(45° - \frac{\phi}{2}\right) - 2c \tan\left(45° - \frac{\phi}{2}\right) + \gamma_w \left(H - H_w\right) \tag{C5}$$

where q_1' is the effective earth pressure at tunnel crown; ϕ is the effective friction angle of soil; c is the effective cohesion of soil; γ_w is the unit weigh of ground water; H is the embedded depth of the tunnel; and, H_w is the ground water table below the ground surface.

(4) Additional lateral earth pressure at tunnel bottom, p_4:

$$p_4 = 2(\gamma_s - \gamma_w) R \tan^2\left(45° - \frac{\phi}{2}\right) + 2\gamma_w R \quad \text{(C6)}$$

where γ_s is the averaged total unit weight of the soil layers from tunnel bottom to tunnel crown.

(5) Averaged self-weight or dead load of the tunnel lining, p_5:

$$p_5 = \gamma_c t \quad \text{(C7)}$$

(6) Lateral soil resistance pressure, p_6, which is assumed as distributed over the range of 45°~135° with respect to the vertical direction around the tunnel, and normal to tunnel lining with a parabolic pattern, defined as:

$$p_6 = p_h\left(1 - 2\cos^2\varphi\right) \quad \left(\frac{\pi}{4} \le \varphi \le \frac{3\pi}{4}\right) \quad \text{(C8)}$$

where p_h is the maximum soil resistance at tunnel springline; and φ is the angle measured from the vertical direction around the tunnel. The Winkler elastic foundation is often employed, which is expressed as

$$p_h = k_h \Delta_h \quad \text{(C9)}$$

where k_h is the horizontal ground stiffness of soil; and Δ_h is the horizontal displacement at tunnel springline.

(7) The additional load on the segment ring due to the shearing effect, p_s, is expressed as:

$$p_s = \frac{R^2 t \sin\varphi}{I_L} \Delta Q_L \quad \text{(C10)}$$

where ΔQ_{L} is the longitudinal shear force increment per unit length caused by the tunnel longitudinal behavior; and I_L is the inertia moment of the tunnel cross-section in the context of tunnel longitudinal behavior analysis, defined as:

$$I_L = \frac{\pi}{4}\left[\left(R+\frac{t}{2}\right)^4 - \left(R-\frac{t}{2}\right)^4\right] \tag{C11}$$

(8) The additional load on the segment ring due to the flattening effect, p_f, is expressed as:

$$p_f = \frac{M_{\mathrm{L}}}{I_{\mathrm{L}}}\kappa R t \cos\varphi \tag{C12}$$

where M_{L} is the longitudinal moment of the shield tunnel caused by the tunnel longitudinal behavior; and κ is the curvature of tunnel settlement, which can be computed with the tunnel settlement curve.

Lists of Tables

List of Figures

Table 1. Statistical characterization of noise factors

Noise factors	Range [a]	Mean (μ) [b]	Coefficient of variation (δ) [b]	Scale of fluctuation (r) [c]	Distribution [d]
Vertical ground stiffness of the ground under the tunnel (k_v, kN/m^3)	–	33,000	0.50	50	Lognormal
Effective cohesion of soil (c, kN/m^2)	0 ~ 15	7.5	0.33	50	Lognormal
Effective friction angle of soil (ϕ, °)	30.0 ~ 35.3	32.65	0.03[e]	50	Lognormal
Horizontal ground stiffness of soil (k_h, kN/m^3)	3,500 ~ 15,000	9250	0.21	50	Lognormal
Ground water table (H_w, m)	0.5 ~ 2.0	1.25	0.20	50	Lognormal
Ground surcharge (q_0, kN/m^2)	0 ~ 20	10	0.33	50	Lognormal

[a] Data obtained from Gong et al. (2014b).
[b] Data estimated with three-sigma rule.
[c] Data obtained from Phoon and Kulhawy (1999).
[d] Data assumed based on engineering experience.
[e] The coefficient of variation (COV) of the effective friction angle is typically in the range of 3% to 7%. Here, the COV is estimated based on the three-sigma rule with the range given by Gong et al. (2014b).

Table 2. Deterministic parameters of the example tunnel

Category	Parameter	Value
Soil	Unit weight (γ_s, kN/m^3)	18.0
Tunnel geometries	Longitudinal length (L, m)	300.0
	Embedded depth (H, m)	14.0
	Tunnel inner radius (R_{in}, m)	2.75
	With of segment ring (b, m)	1.0
	Position of circumferential joints of half structure (φ_i, °)	8, 73, 138
Tunnel segment	Unit weight of concrete (γ_c, kN/m^3)	25.0
	Elastic modulus of concrete (E_c, kN/m^2)	34.5×10^6
	Compression strength of concrete (f_c, kN/m^2)	39×10^3
	Ultimate plastic strain of concrete (ε_p)	0.0033
Steel reinforcement	Elastic modulus of steel (E_s, kN/m^2)	210×10^6
	Yielding strength of steel (f_y, kN/m^2)	345×10^3
	Thickness of protective concrete cover (a, m)	0.05
Steel bolt	Length of steel bolts (l_b, m)	0.4
	Number of bolts at each circumferential joint	2
	Distance from bolts center to tunnel inside surface (h)	t/3
	Number of steel bolts between adjacent segment rings (or of each longitudinal joint)	17

Table 3. Design space of the robust design of the example tunnel

Easy-to-control design parameter	Possible value
Segment thickness (t: m)	{0.25, 0.30, 0.35, 0.40, 0.45}
Steel reinforcement ratio of tunnel segment (ρ: %)	{0.5, 1.0, 1.5, 2.0}
Bolt diameter of the circumferential joints (D_c: mm)	{20, 25, 30, 35, 40}
Bolt diameter of the longitudinal joints (D_l: mm)	{20, 25, 30, 35, 40}

Table 4. Comparison between the knee point in robust design and the actual design

Designs	Easy-to-control design parameters (***d***)				Design feasibility		Tunnel performance		Design objectives		
	t (m)	ρ (%)	D_c (mm)	D_l (mm)	f_1	f_2	Mean of μ_{Fs1}	Mean of μ_{Fs2}	*Cost, C* (1000 USD)	*Robustness* R_1	*Robustness* R_2
Knee point	0.35	0.5	20	30	0.9607	0.9033	1.90	1.80	309.57	9.59	4.89
Actual design	0.35	0.5	30	30	0.7846	0.9695	1.39	2.50	316.67	8.78	2.31

Table 5. Robust design optimization results of the example tunnel with different target factors of safety

Target factors of safety	Easy-to-control design parameters (***d***)				Design feasibility		Tunnel performance		Number of non-dominated optimal designs	Design objectives		
	t (m)	ρ (%)	D_c (mm)	D_l (mm)	f_1	f_2	Mean of μ_{Fs2}	Mean of μ_{Fs2}		C (1000 USD)	R_1	R_2
1.5	0.35	0.50	20	30	0.9607	0.9033	1.90	1.80	71	309.57	9.59	4.89
2.0	0.40	0.50	20	30	0.9931	0.9643	2.12	2.10	47	353.18	11.09	4.61
2.5	0.40	1.00	25	35	0.9999	0.9963	3.39	2.53	42	474.85	10.76	4.59
3.0	0.45	1.00	25	35	1.0000	0.9997	3.94	3.04	17	534.22	11.74	4.34

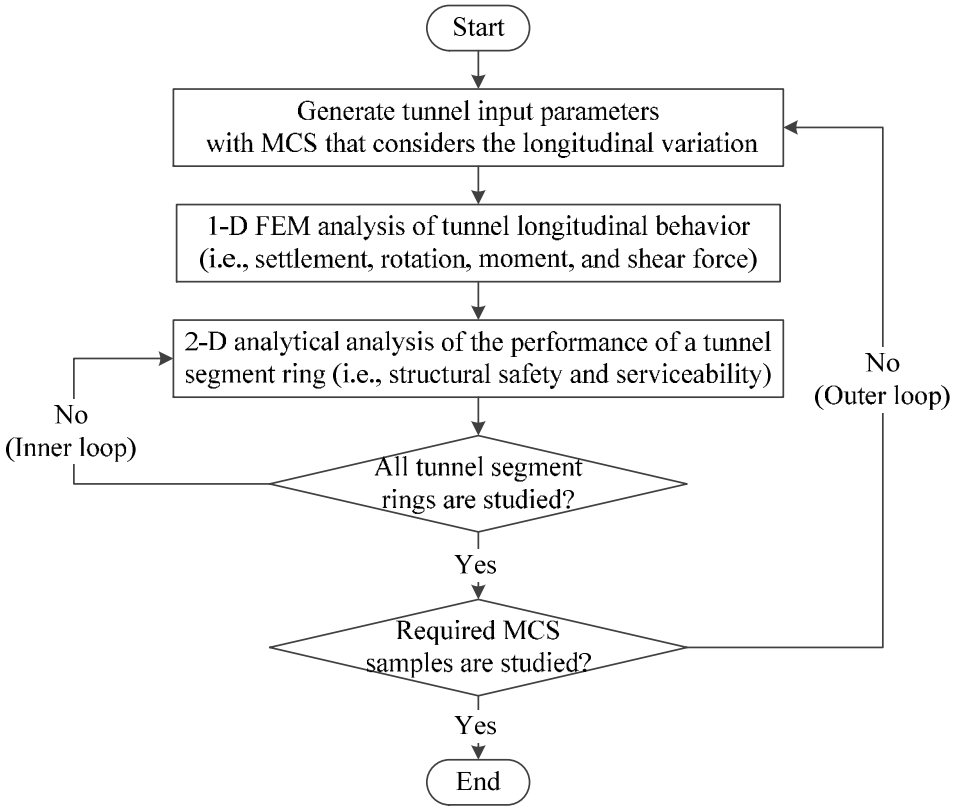

Figure 1. Framework for shield tunnel performance analysis

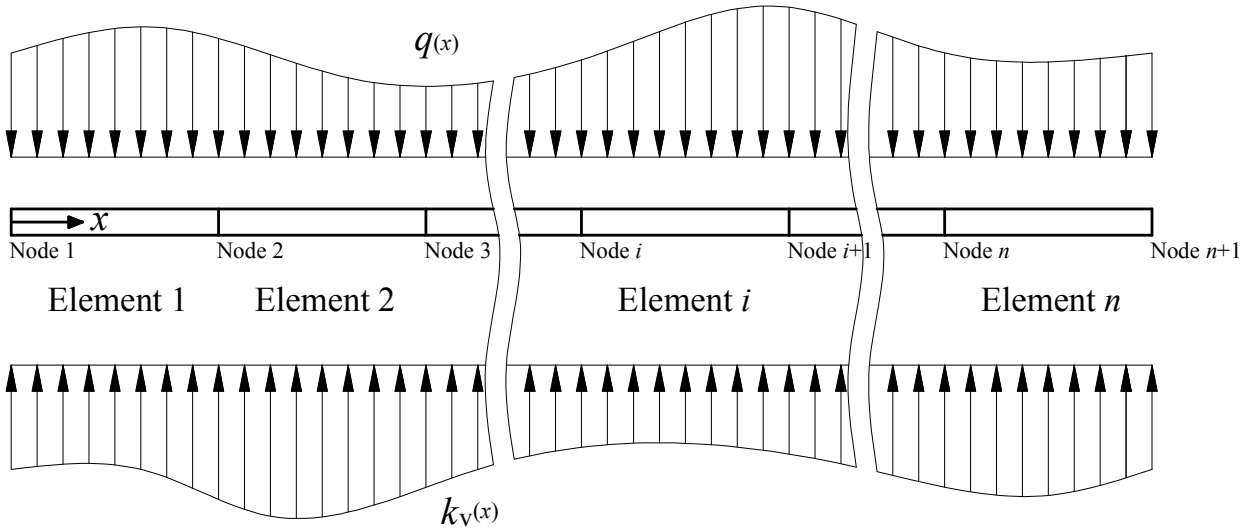

Figure 2. Schematic diagram of 1-D FEM solution of tunnel longitudinal behavior

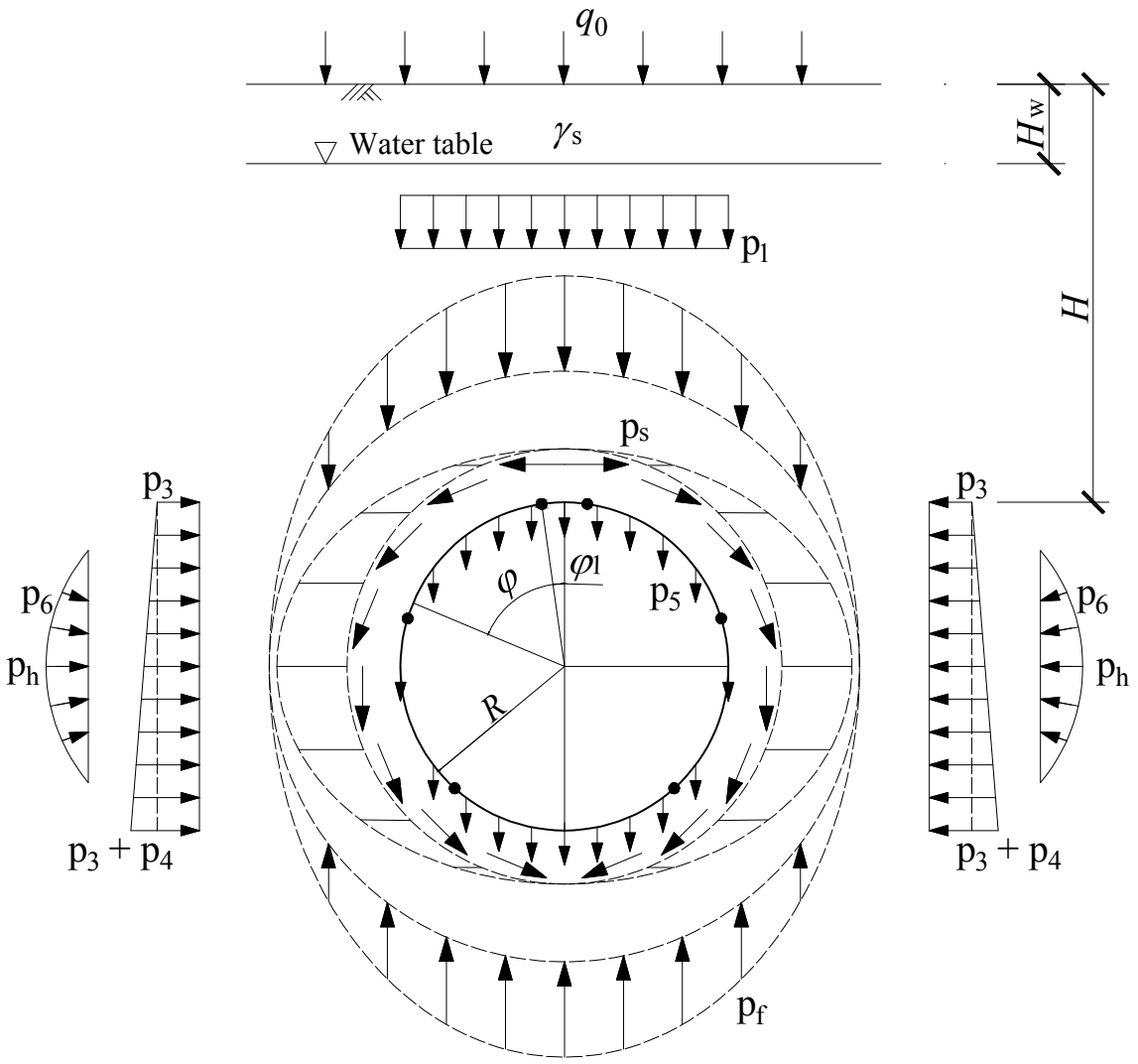

Figure 3. Schematic diagram of 2-D analytical solution of the performance of the segment ring

Find:	$\boldsymbol{d}$ ($\boldsymbol{d}$ denotes a set of easy-to-control design parameters)
Subject to:	$\boldsymbol{d} \in \mathbf{DS}$ (**DS** denotes the design pool)
	$g(\boldsymbol{d}, \boldsymbol{\theta}) > 0$ ($g > 0$ denotes the performance requirement)
Objectives:	minimize $C(\boldsymbol{d})$ (C denotes the cost)
	maximize $R(\boldsymbol{d}, \boldsymbol{\theta})$ (R denotes the design robustness)

Figure 4. Multi-objective optimization setting for robust design

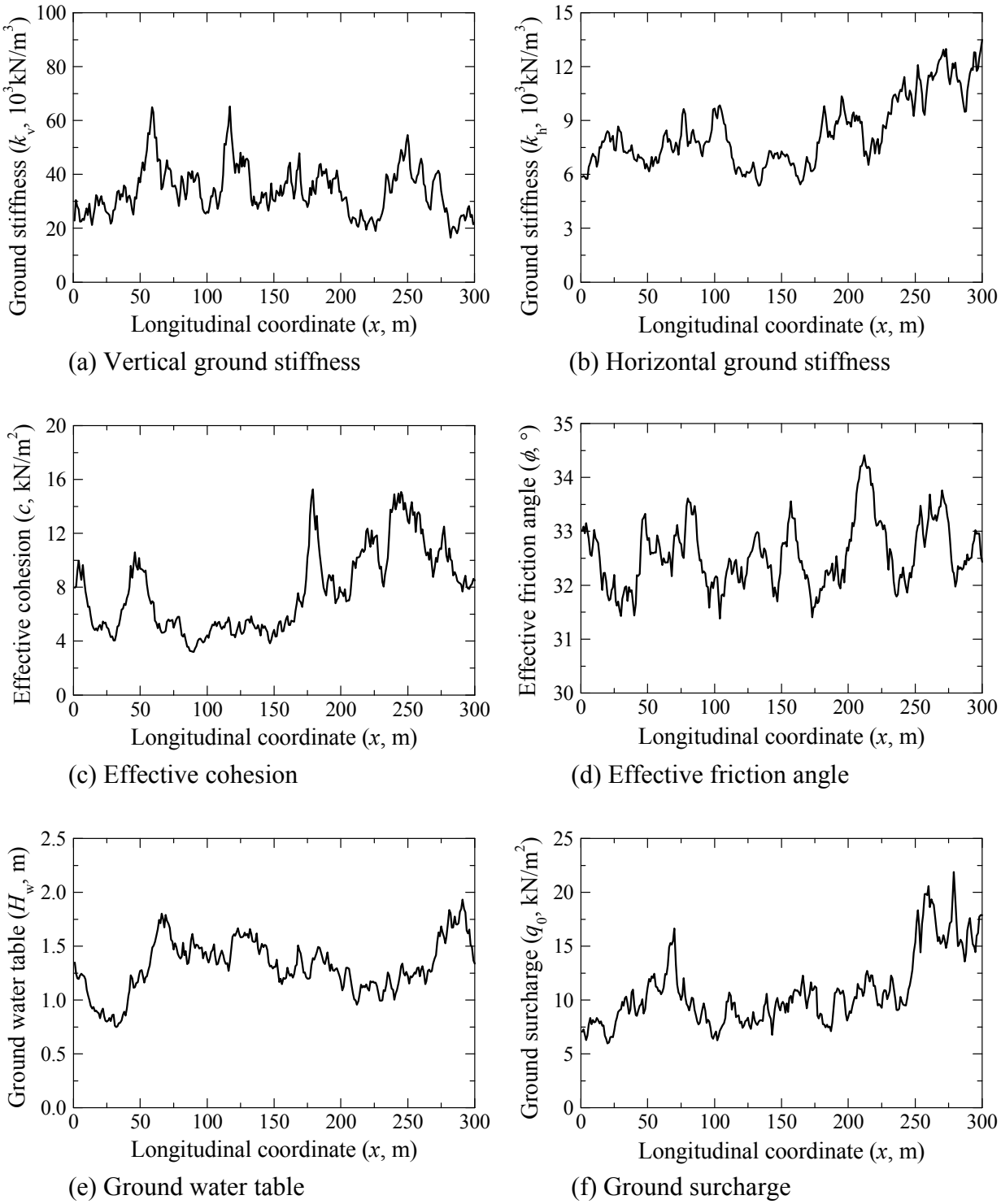

Figure 5. Illustrative longitudinal variation of noise factors

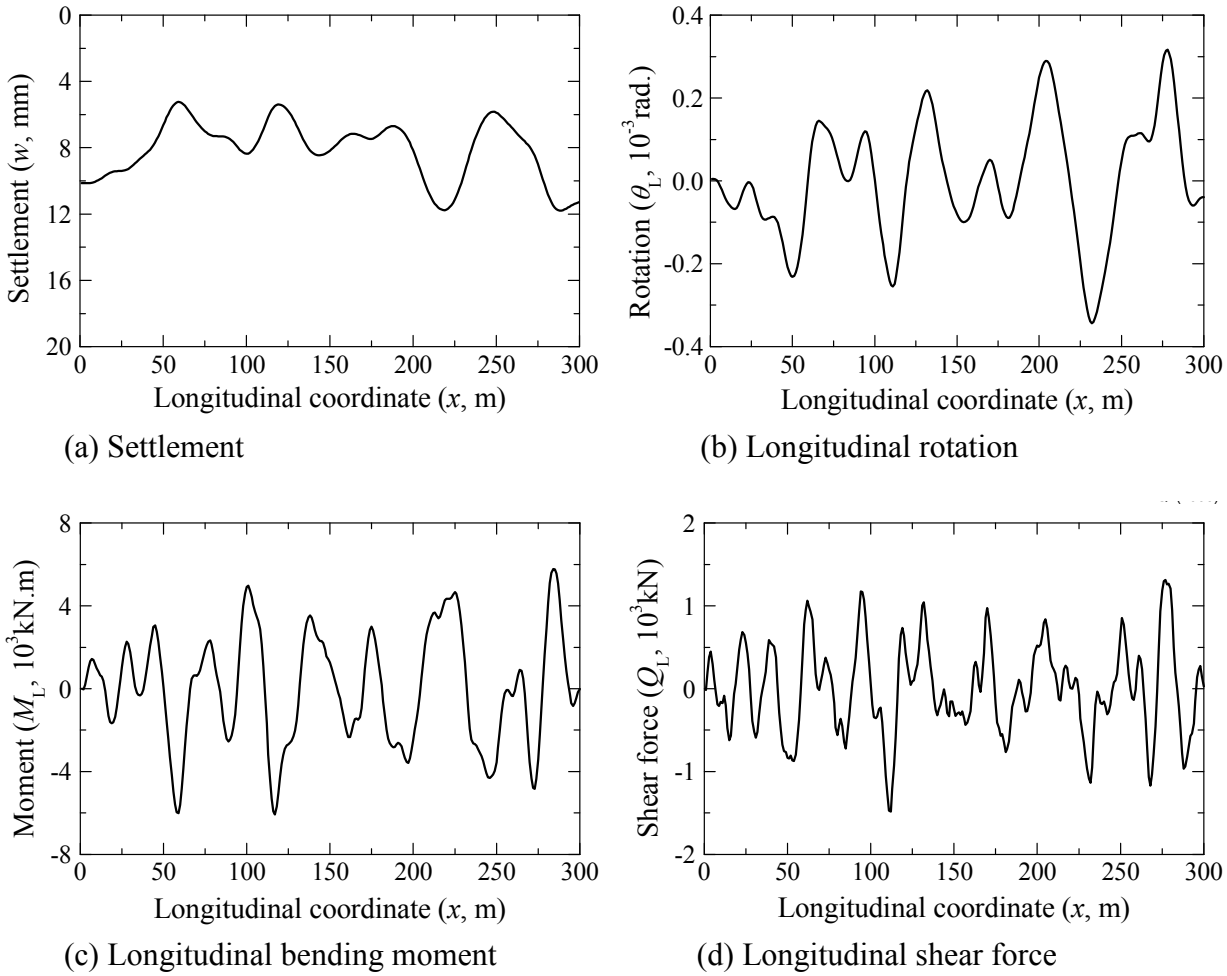

Figure 6. Computed tunnel longitudinal behaviors given the noise factors in Figure 5

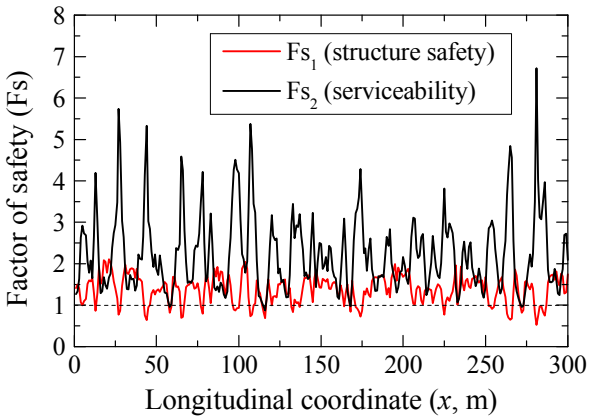

Figure 7. Computed tunnel performance given the noise factors in Figure 5

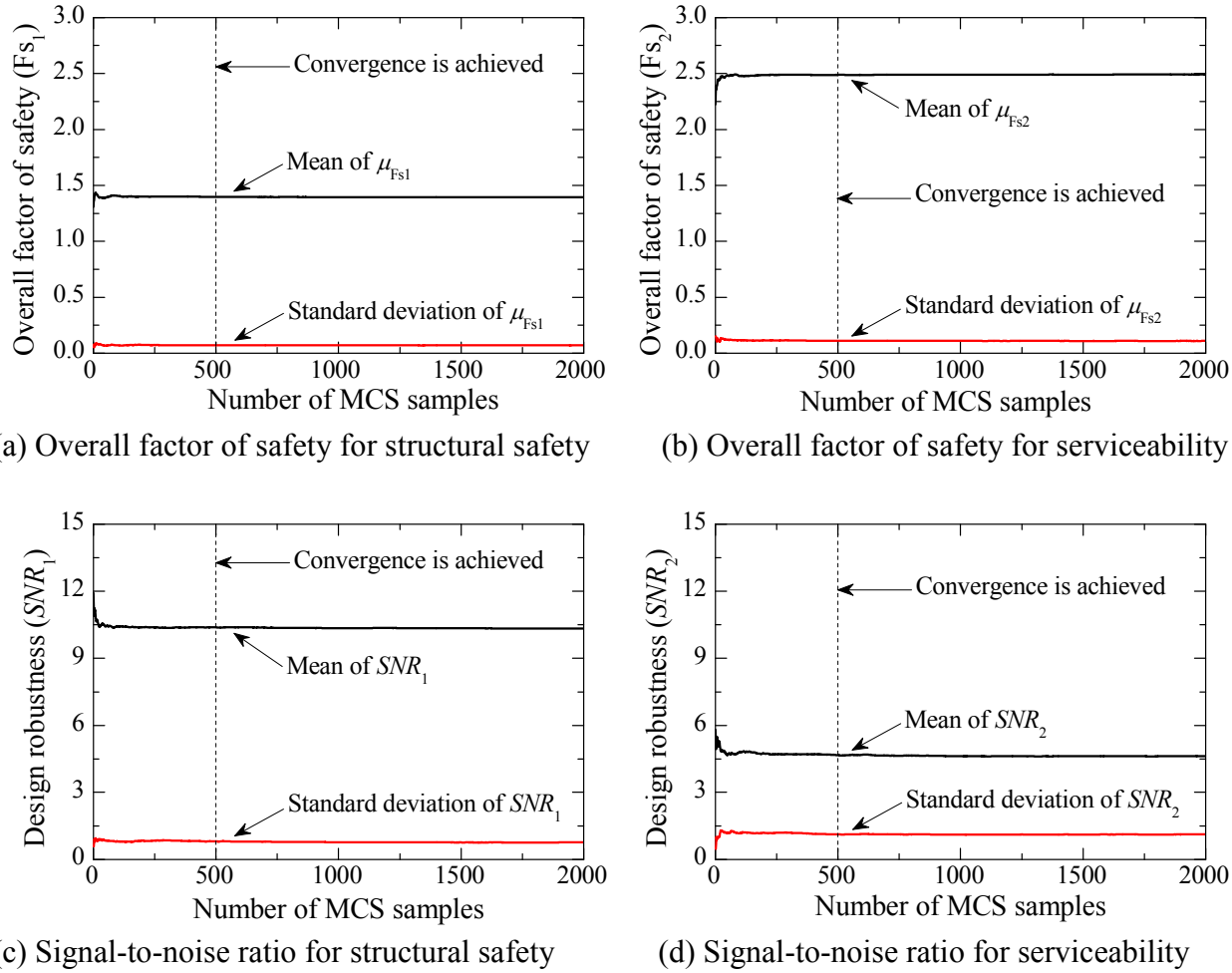

(a) Overall factor of safety for structural safety

(b) Overall factor of safety for serviceability

(c) Signal-to-noise ratio for structural safety

(d) Signal-to-noise ratio for serviceability

Figure 8. Convergence of the overall factors of safety and signal-to-noise ratio with number of MCS samples

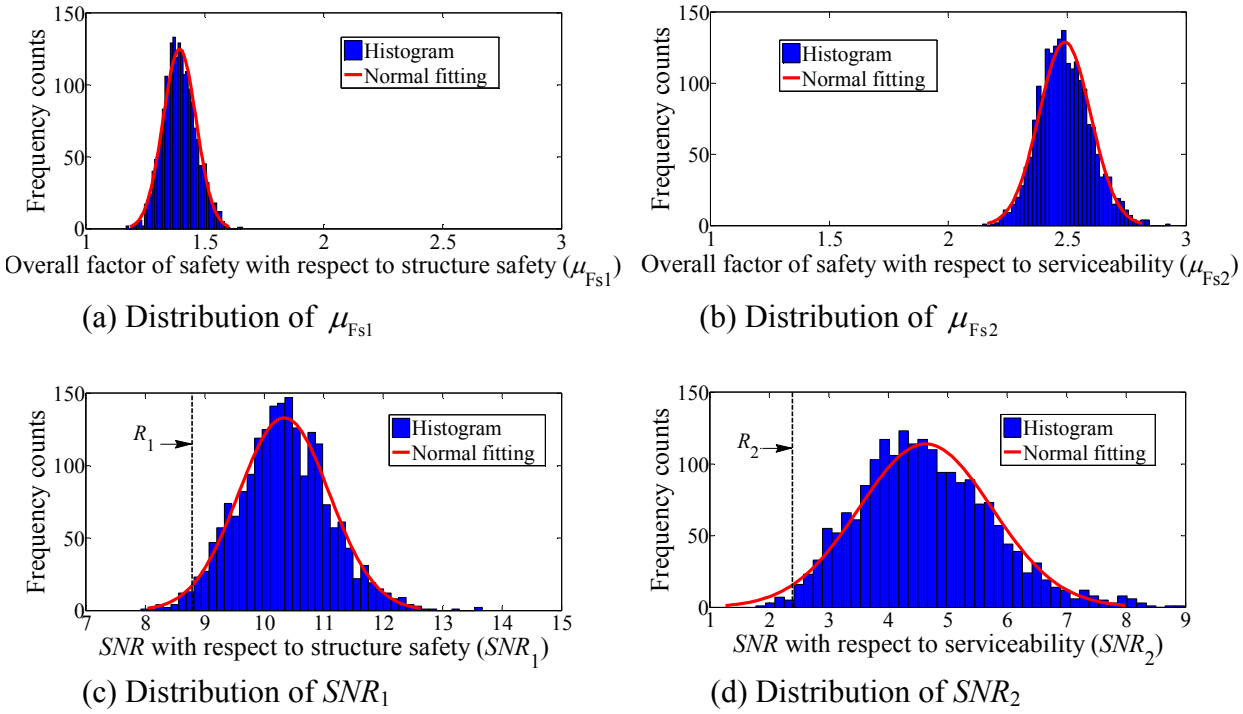

Figure 9. Distributions of the overall factors of safety and *SNR* in 2,000 MCS runs

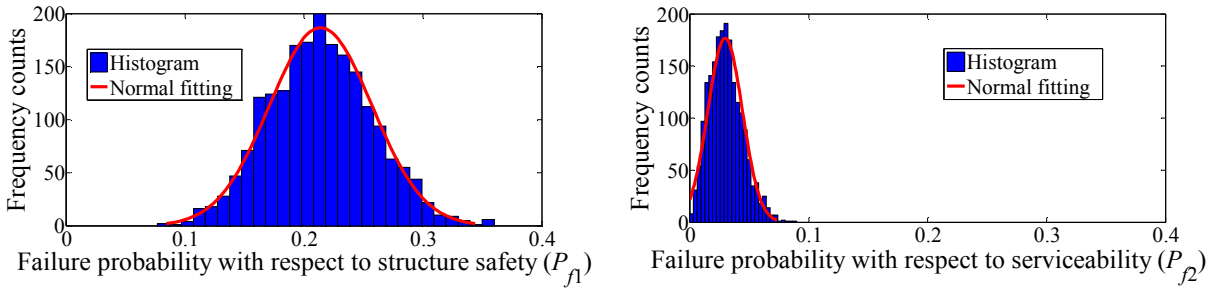

(a) Failure probability for structural safety (b) Failure probability for serviceability

Figure 10. Failure probabilities in 2,000 MCS runs using the proposed framework for shield tunnel performance analysis

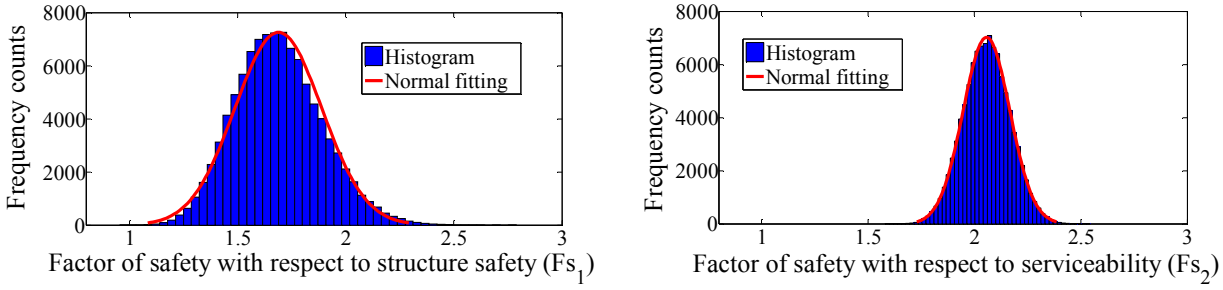

(a) Factor of safety for structural safety

(b) Factor of safety for serviceability

Figure 11. Factors of safety in 100,000 MCS runs using the conventional methods for shield tunnel performance analysis

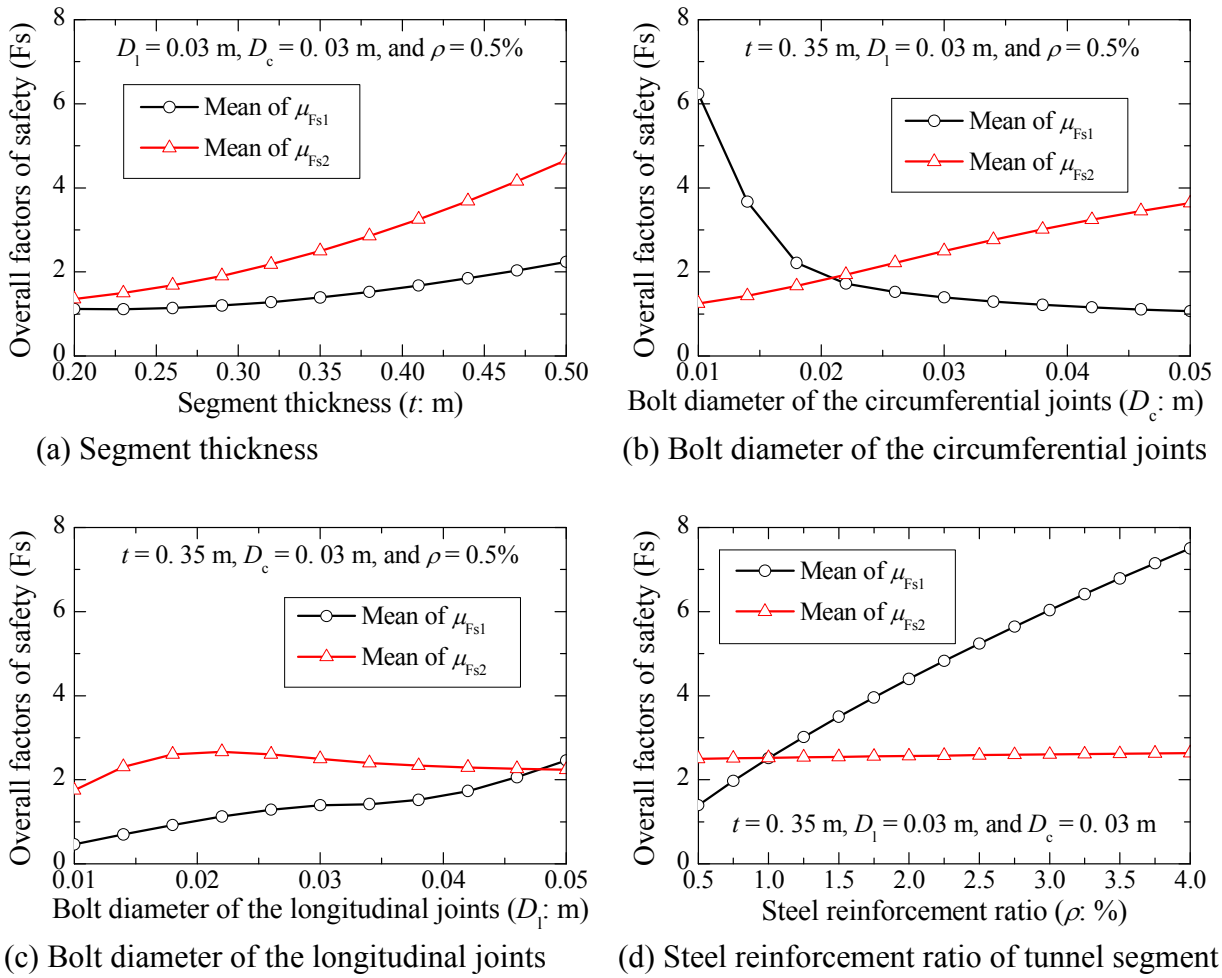

(a) Segment thickness

(b) Bolt diameter of the circumferential joints

(c) Bolt diameter of the longitudinal joints

(d) Steel reinforcement ratio of tunnel segment

Figure 12. Effects of easy-to-control design parameters on tunnel performance

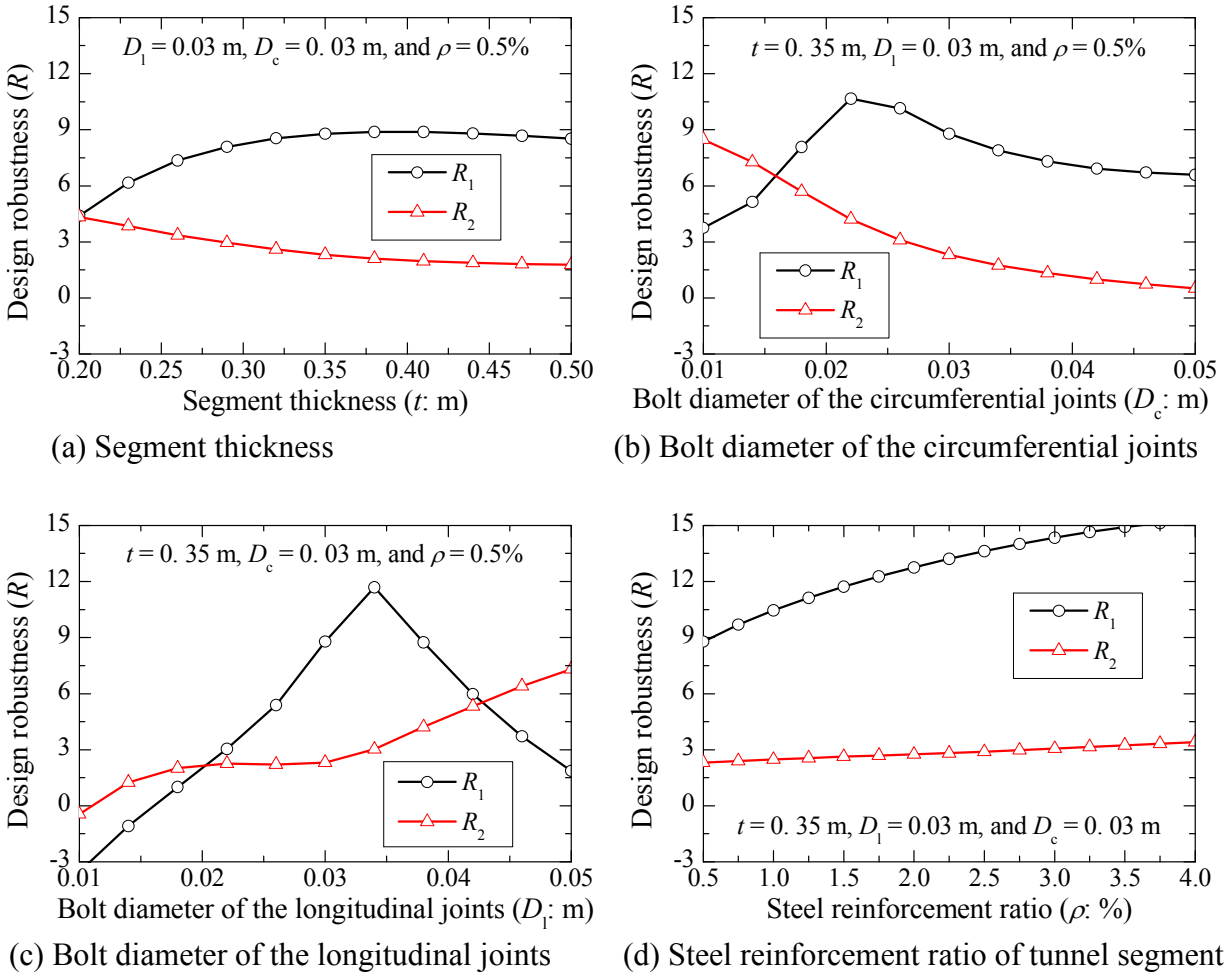

(a) Segment thickness

(b) Bolt diameter of the circumferential joints

(c) Bolt diameter of the longitudinal joints

(d) Steel reinforcement ratio of tunnel segment

Figure 13. Effects of easy-to-control design parameters on design robustness

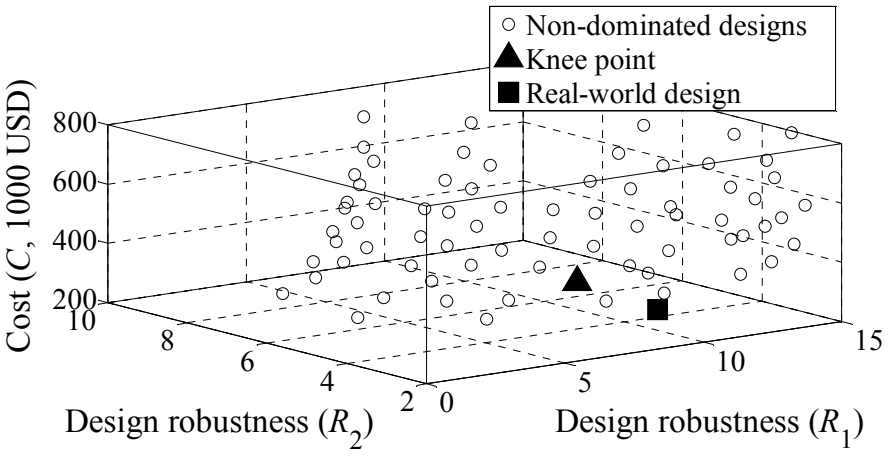

Figure 14. Robust design optimization results of the example tunnel